



# GeV Variability Properties of TeV Blazars Detected by Fermi-LAT

Gege Wang<sup>1</sup> , Hubing Xiao<sup>2</sup> , Junhui Fan<sup>3,4</sup> , and Xin Zhang<sup>1,5,6</sup> <sup>1</sup> Key Laboratory of Cosmology and Astrophysics (Liaoning) & College of Sciences, Northeastern University, Shenyang 110819, People's Republic of China; [wanggege@mail.neu.edu.cn](mailto:wanggege@mail.neu.edu.cn), [zhangxin@mail.neu.edu.cn](mailto:zhangxin@mail.neu.edu.cn)<sup>2</sup> Shanghai Key Lab for Astrophysics, Shanghai Normal University, Shanghai, 200234, People's Republic of China<sup>3</sup> Center for Astrophysics, Guangzhou University, Guangzhou 510006, People's Republic of China; [fjh@gzhu.edu.cn](mailto:fjh@gzhu.edu.cn)<sup>4</sup> Astronomy Science and Technology Research Laboratory of Department of Education of Guangdong Province, Guangzhou 510006, People's Republic of China<sup>5</sup> National Frontiers Science Center for Industrial Intelligence and Systems Optimization, Northeastern University, Shenyang 110819, People's Republic of China<sup>6</sup> Key Laboratory of Data Analytics and Optimization for Smart Industry (Northeastern University), Ministry of Education, Shenyang 110819, People's Republic of China

Received 2023 June 27; revised 2023 October 30; accepted 2023 October 30; published 2024 January 19

## Abstract

Variability is a prominent observational feature of blazars. The high-energy radiation mechanism of jets has always been important but is still unclear. In this work, we performed a detailed analysis using Fermi-LAT data across 15 yr and obtained GeV light-curve information for 78 TeV blazars detected by Fermi. We provided annual GeV fluxes and corresponding spectral indices for the 78 TeV blazars and thorough monthly GeV fluxes for a subsample of 41 bright blazars. Our results suggest a strong correlation between the  $\gamma$ -ray photon index and  $\log L_\gamma$  for the flat spectrum radio quasars (FSRQs) and high-energy peaked BL Lacs. Fourteen sources in our sample show significant GeV outbursts/flares above the relatively stable, low-flux light curve, with six of them showing a clear sharp peak profile in their 5 day binned light curves. We quantified the variability utilizing the fractional variability parameter  $F_{\text{var}}$ , and found that the flux of the FSRQs showed significantly stronger variability than that of the BL Lacs. The 41 bright blazars in this work are best fit by a log-normal flux distribution. We checked the spectral behavior and found 11 out of the 14 sources show a *bluer-when-brighter* trend, suggesting this spectral behavior for these TeV blazars at the GeV band arises from the mechanism in which the synchrotron-self Compton process dominates the GeV emission. Our research offers a systematic analysis of the GeV variability properties of TeV blazars and serves as a helpful resource for further associated blazar studies.

*Unified Astronomy Thesaurus concepts:* [Relativistic jets \(1390\)](#); [Active galactic nuclei \(16\)](#); [Gamma-ray observatories \(632\)](#)

*Supporting material:* figure sets, machine-readable tables

## 1. Introduction

Blazars are the most powerful active galactic nuclei (AGNs) sources, which show very extreme observational properties, including variability over almost the whole electromagnetic wave band, high and variable polarization, strong  $\gamma$ -ray emissions, and apparent superluminal motion, which are believed to be associated with a relativistic beaming effect of the jet (Urry & Padovani 1995; Villata et al. 2006; Fan et al. 2014; Gupta et al. 2016; Xiao et al. 2019, 2022b; Fan et al. 2021). Blazars are usually divided into two subclasses: flat spectrum radio quasars (FSRQs) with strong emission lines, and BL Lacertae objects (BL Lacs) that have weak or even no emission lines (Scarpa & Falomo 1997). The broadband emission of blazars ranges from the radio band to very high energy (VHE), which is generally dominated by nonthermal radiation. The broadband spectral energy distribution of a blazar shows two humps, and it is generally accepted that the lower energy hump peak is dominated by the synchrotron mechanism. The higher energy hump peak could be produced by inverse Compton (IC) scattering of synchrotron photons (synchrotron-self Compton (SSC), Bloom & Marscher 1996; Finke et al. 2008) and external photons (external Compton,

Sikora et al. 1994; Kang et al. 2014) in the framework of leptonic models. Meanwhile, the hadronic model suggests that the higher energy hump is attributed to the proton synchrotron radiation and secondary particle cascade (Mücke & Protheroe 2001; Dimitrakoudis et al. 2012; Cerruti et al. 2015; Diltz et al. 2015; Xue et al. 2021; Wang et al. 2022c). The hadronic model seems to be promising following the detection of extragalactic neutrino events from the blazar TXS 0506+056 (IceCube Collaboration et al. 2018a).

The discovery of the first TeV blazar, Mrk 421, was a surprise when it was detected by the Whipple telescope in 1992 because it could barely be seen in the  $\gamma$ -ray band (Punch et al. 1992). The following detection of more TeV blazars, e.g., Mrk 501, 1ES 2344+514, and PKS 2155-304 (Quinn et al. 1996; Catanese et al. 1998; Chadwick et al. 1999), started the era of the study TeV blazars. There are 252 sources associated with TeV emission, and 81 of them are confirmed as blazars according to TeVCat<sup>7</sup>, the detection of TeV emissions mainly relies on ground-based Cherenkov telescopes, e.g., the Major Atmospheric Gamma Imaging Cherenkov telescope (MAGIC), High Energy Stereoscopic System telescope (H. E. S. S.), and Very Energetic Radiation Imaging Telescope Array System (VERITAS). Our understanding of blazar TeV emission is limited by several issues, e.g., the sample size of TeV blazars, the lack of TeV light curves due to the observation mode of Cherenkov telescopes, the effective absorption of extragalactic

**Table 1**  
Sample of TeV Blazars

4FGL Name (1)	Association (2)	$z$ (3)	Class (4)	$F_{\gamma}/10^{-11}$ (erg · cm <sup>-2</sup> · s <sup>-1</sup> ) (5)	$\Gamma$ ( $\alpha$ ) (6)
J0013.9-1854	SHBL J001355.9-185406	0.094	IBL	0.2 ± 0.03	2.05 ± 0.13
J0033.5-1921	KUV 00311-1938	0.61	HBL	222.4 ± 11.1	1.47 ± 0.07
J0035.9+5950	1ES 0033+595	0.086	HBL	56.6 ± 1.8	1.53 ± 0.02
J0112.1+2245	S2 0109+22	0.265	IBL	43.6 ± 2.2	1.96 ± 0.07
J0136.5+3906	RGB J0136+391	0.75	HBL	318.9 ± 9.8	1.34 ± 0.05
J0152.6+0147	RGB J0152+017	0.08	IBL	0.7 ± 0.06	1.96 ± 0.07
J0214.3+5145	TXS 0210+515	0.049	HBL	0.5 ± 0.05	1.9 ± 0.09
J0221.1+3556	S3 0218+35	0.944	FSRQ	5.9 ± 1.1	2.30 ± 0.01
J0222.6+4302	3C 66A	0.34	IBL	62.9 ± 1.5	1.84 ± 0.04
J0232.8+2018	1ES 0229+200	0.139	HBL	0.4 ± 0.06	1.74 ± 0.11
J0238.4-3116	1RXS J023832.6-311658	0.232	HBL	1.3 ± 0.08	1.79 ± 0.05
J0303.4-2407	PKS 0301-243	0.26	IBL	10.8 ± 0.6	1.86 ± 0.07
J0319.8+1845	RBS 413	0.19	HBL	0.8 ± 0.08	1.72 ± 0.08
J0349.4-1159	1ES 0347-121	0.188	HBL	0.6 ± 0.06	1.73 ± 0.09
J0416.9+0105	1ES 0414+009	0.287	HBL	0.7 ± 0.07	1.8 ± 0.08
J0449.4-4350	PKS 0447-439	0.205	HBL	169 ± 3.4	1.67 ± 0.03
J0507.9+6737	1ES 0502+675	0.34	HBL	3.9 ± 0.04	1.54 ± 0.01
J0509.4+0542	TXS 0506+056	0.337	IBL	29.6 ± 1.1	1.98 ± 0.06
J0521.7+2112	VER J0521+211	0.108	HBL	30.7 ± 0.7	1.87 ± 0.04
J0550.5-3216	PKS 0548-322	0.069	HBL	0.4 ± 0.05	1.86 ± 0.1
J0648.7+1516	RX J0648.7+1516	0.179	HBL	2 ± 0.05	1.73 ± 0.02
J0650.7+2503	1ES 0647+250	0.203	HBL	30.1 ± 1	1.59 ± 0.04
J0710.4+5908	RGB J0710+591	0.125	HBL	0.9 ± 0.08	1.62 ± 0.06
J0721.9+7120	S5 0716+714	0.3	IBL	326.3 ± 8.7	1.85 ± 0.03
J0733.4+5152	PGC 2402248	0.065	BCU	0.4 ± 0.02	1.69 ± 0.02
J0739.2+0137	PKS 0736+017	0.189	FSRQ	35.8 ± 4	2.26 ± 0.12
J0809.8+5218	1ES 0806+524	0.138	HBL	15 ± 0.6	1.75 ± 0.06
J0812.0+0237	1RXS J081201.8+023735	0.172	HBL	0.6 ± 0.03	1.83 ± 0.03
J0847.2+1134	RBS 723	0.199	HBL	0.7 ± 0.07	1.7 ± 0.08
J0854.8+2006	OJ 287	0.306	IBL	6.9 ± 0.5	2.18 ± 0.1
J0904.9-5734	PKS 0903-57	0.695	BCU	7 ± 1.7	2.07 ± 0.03
J0958.7+6534	S4 0954+65	0.367	IBL	15 ± 1.2	2.08 ± 0.1
J1010.2-3119	1RXS J101015.9-311909	0.143	HBL	0.9 ± 0.08	1.75 ± 0.07
J1015.0+4926	1ES 1011+496	0.212	HBL	33.4 ± 1.1	1.76 ± 0.05
J1058.6+2817	GB6 J1058+2817	...	IBL	0.7 ± 0.02	2.14 ± 0.02
J1103.6-2329	1ES 1101-232	0.186	HBL	0.8 ± 0.09	1.63 ± 0.08
J1104.4+3812	Mrk 421	0.031	HBL	139.2 ± 1.9	1.67 ± 0.02
J1136.4+6736	RX J1136.5+6737	0.136	HBL	0.7 ± 0.06	1.73 ± 0.06
J1136.4+7009	Mrk 180	0.045	HBL	1.4 ± 0.08	1.79 ± 0.04
J1159.5+2914	TON 599	0.729	FSRQ	18.7 ± 1.3	2.19 ± 0.08
J1217.9+3007	1ES 1215+303	0.13	IBL	54.5 ± 1.7	1.8 ± 0.05
J1221.3+3010	1ES 1218+304	0.182	HBL	6.3 ± 0.2	1.7 ± 0.02
J1221.5+2814	W Comae	0.103	IBL	2.1 ± 0.09	2.19 ± 0.04
J1224.4+2436	MS 1221.8+2452	0.219	IBL	1.1 ± 0.07	1.95 ± 0.05
J1224.9+2122	4C 21.35	0.435	FSRQ	31.2 ± 2.5	2.23 ± 0.08
J1230.2+2517	S3 1227+25	0.135	IBL	32.3 ± 2.2	1.95 ± 0.09
J1256.1-0547	3C 279	0.536	FSRQ	456.1 ± 20.3	2.1 ± 0.05
J1315.0-4236	1ES 1312-423	0.105	HBL	0.7 ± 0.08	1.69 ± 0.09
J1422.3+3223	B2 1420+32	0.682	FSRQ	122.2 ± 0.4	1.94 ± 0.02
J1427.0+2348	PKS 1424+240	0.16	IBL	196.3 ± 5.3	1.62 ± 0.04
J1428.5+4240	H1426+428	0.129	HBL	1.3 ± 0.09	1.62 ± 0.05
J1442.7+1200	1ES 1440+122	0.163	HBL	0.8 ± 0.08	1.7 ± 0.07
J1443.9+2501	PKS 1441+25	0.939	FSRQ	241.8 ± 17	1.85 ± 0.1
J1443.9-3908	PKS 1440-389	0.065	HBL	60.9 ± 2.1	1.65 ± 0.05
J1512.8-0906	PKS 1510-089	0.36	FSRQ	35.6 ± 1	2.38 ± 0.04
J1517.7-2422	AP Lib	0.048	IBL	13.8 ± 0.5	2.01 ± 0.02
J1518.0-2731	TXS 1515-273	0.128	LBL	1.4 ± 0.08	2.05 ± 0.05
J1555.7+1111	PG 1553+113	0.36	HBL	721.2 ± 12.6	1.43 ± 0.03
J1653.8+3945	Mrk 501	0.034	HBL	22.2 ± 0.5	1.74 ± 0.04
J1725.0+1152	H 1722+119	0.018	HBL	82.5 ± 3	1.65 ± 0.05
J1728.3+5013	1ES 1727+502	0.055	HBL	2.3 ± 0.1	1.77 ± 0.03
J1744.0+1935	1ES 1741+196	0.084	HBL	0.8 ± 0.06	1.93 ± 0.06
J1751.5+0938	OT 81	0.322	LBL	20.2 ± 1.4	2.13 ± 0.09

**Table 1**  
(Continued)

4FGL Name (1)	Association (2)	$z$ (3)	Class (4)	$F_\gamma/10^{-11}$ (erg · cm <sup>-2</sup> · s <sup>-1</sup> ) (5)	$\Gamma$ ( $\alpha$ ) (6)
J1813.5+3144	B2 1811+31	0.117	IBL	0.5 ± 0.3	1.93 ± 0.08
J1857.9+0313c	MAGIC J1857.6+0297	...	BCU	0.6 ± 0.1	3.15 ± 0.29
J1944.0+2117	HESS J1943+213	...	HBL	2.2 ± 0.3	1.34 ± 0.14
J2000.0+6508	1ES 1959+650	0.047	HBL	28.1 ± 0.6	1.74 ± 0.03
J2001.2+4353	MAGIC J2001+435	0.174	IBL	49.9 ± 2	1.78 ± 0.07
J2009.4-4849	PKS 2005-489	0.071	HBL	5.6 ± 0.3	1.82 ± 0.09
J2039.5+5218	1ES 2037+521	0.053	IBL	0.7 ± 0.08	1.77 ± 0.09
J2056.7+4939	RGB J2056+496	...	BCU	2.2 ± 0.04	1.85 ± 0.01
J2158.8-3013	PKS 2155-304	0.116	HBL	116.6 ± 2.4	1.72 ± 0.03
J2202.7+4216	BL Lacertae	0.069	IBL	72.2 ± 1.8	2.11 ± 0.04
J2243.9+2021	RGB J2243+203	0.39	IBL	65.5 ± 2.5	1.71 ± 0.06
J2250.0+3825	B3 2247+381	0.119	IBL	1 ± 0.08	1.72 ± 0.06
J2324.7-4041	1ES 2322-409	0.174	HBL	11.8 ± 0.8	1.61 ± 0.09
J2347.0+5141	1ES 2344+514	0.044	HBL	3.3 ± 0.1	1.88 ± 0.04
J2359.0-3038	H 2356-309	0.165	HBL	0.6 ± 0.06	1.79 ± 0.08

**Note.** Here we use the classification reported in Fan et al. (2016). Low-energy peaked BL Lacs (LBL): for BL Lacs with the synchrotron peak frequency  $\log \nu_p$  (Hz)  $\leq$  14.0; intermediate-energy-peaked BL Lacs (IBL):  $14.0 < \log \nu_p$  (Hz)  $\leq$  15.3; high-energy peaked BL Lacs (HBL):  $\log \nu_p$  (Hz)  $>$  15.3.  $F_\gamma$  and  $\Gamma_\gamma^{\text{ph}}$  are the 1–300 GeV energy flux and photon index of the maximum likelihood analysis results over 15 yr, respectively.

(This table is available in machine-readable form.)

background light. A multiwavelength study is usually employed to investigate the emission properties of TeV blazars; however, this method can only be applied to several individual sources. Otherwise, we can also study this subject at other bands, for instance, the GeV  $\gamma$ -ray band.

The Fermi-Large Area Telescope (LAT), first launched in 2008, scans the entire sky every 3 hr, in the range of 20 MeV to above 300 GeV (Atwood et al. 2009). During the last 15 yr, five generations of Fermi catalogs have been released with the latest one being the Fermi-LAT 14-Year Point Source Catalog (4FGL-DR4; Abdollahi et al. 2020). More than 5000 sources have been observed, about 60% of which are confirmed as blazars and blazars have been established to be the dominant  $\gamma$ -ray sources in the extragalactic sky (Ackermann et al. 2015; Ajello et al. 2020). Based on these observations, significant progress has been made in blazar studies, e.g., the classification that depends on the synchrotron peak frequency (Abdo et al. 2010a; Fan et al. 2016; Yang et al. 2022), the *blazar sequence* (Fan et al. 2017; Ghisellini et al. 2017; Ouyang et al. 2023), and the blazar central engine (Paliya et al. 2021; Xiao et al. 2022a). More studies focus on individual sources, study the properties of flares or outbursts, and put constraints on the blazar emission mechanism, such as the flare of 3C 279 (Shukla & Mannheim 2020; Wang et al. 2022a; Tolamatti et al. 2022), the neutrino TXS 0506+056 (IceCube Collaboration et al. 2018b), variability and spectral properties for 3C 279, Ton 599, and PKS 1222+216 (Adams et al. 2022), and the light-curve study of PKS 1510+089 (Prince et al. 2017) to obtain information on blazar emission variability, periodicity, and spectrum. Long-coverage observations on different timescales and spectral analysis can be carried out by taking advantage of the all-sky monitoring capabilities of Fermi-LAT. Recently, the Fermi-LAT Light Curve Repository (LCR), which provides a publicly available, continually updated library of gamma-ray light curves of Fermi sources, was released (Abdollahi et al. 2023). However, this library provides light curves binned only on timescales of 3, 7, and 30 days based on the Fermi-LAT 10-Year Source Catalog (4FGL-DR2; Ballet et al. 2020).

In this work, we aim to provide detailed GeV  $\gamma$ -ray variability information for the TeV blazars based on 15 yr of Fermi-LAT 12-year Source Catalog (4FGL-DR3) data. We described the sample selection and Fermi data analysis in Section 2. The results are reported in Section 3. A discussion and conclusions are presented in Sections 4 and 5, respectively.

## 2. Data Analysis

### 2.1. Sample Selection

We collected 78 blazars, including 66 BL Lacs, eight FSRQs, and four blazar candidates of uncertain type (BCUs) by cross-matching TeVCat with the latest 4FGL-DR3 catalog (Abdollahi et al. 2022). These sources are listed in Table 1, in which columns (1) and (2) list the source 4FGL name and associated name; column (3) lists the redshift obtained from Chen (2018); column (4) lists the classification that is determined based on the synchrotron peak frequency information and criterion in Fan et al. (2016). We also show the redshift distribution of each type of these blazars in Figure 1.

### 2.2. Fermi-LAT Observations and Data Reduction

LAT is one of the main instruments on board Fermi. LAT scans the whole sky every 3 hr in the energy range of 20 MeV to  $>$ 300 GeV (Atwood et al. 2009). We selected LAT data from the Fermi Pass 8 database for the time period from 2008 August 4 15:43:36 (UTC) to 2023 March 9 03:03:00 (UTC), with an energy range of 1–300 GeV. Following the recommendations of the LAT team,<sup>8</sup> we selected events with zenith angles less than 90° to prevent possible contamination from the Earth’s limb. The LAT science tool *Fermitools* 2.0.8 and the instrument response function *P8R3\_SOURCE\_V2* were used. For the selected samples, a 20° × 20° square region of interest (ROI) centered at their positions given in 4FGL-DR3 was selected. The normalization parameters and spectral indices of

<sup>8</sup> <http://fermi.gsfc.nasa.gov/ssc/data/analysis/scitools/>

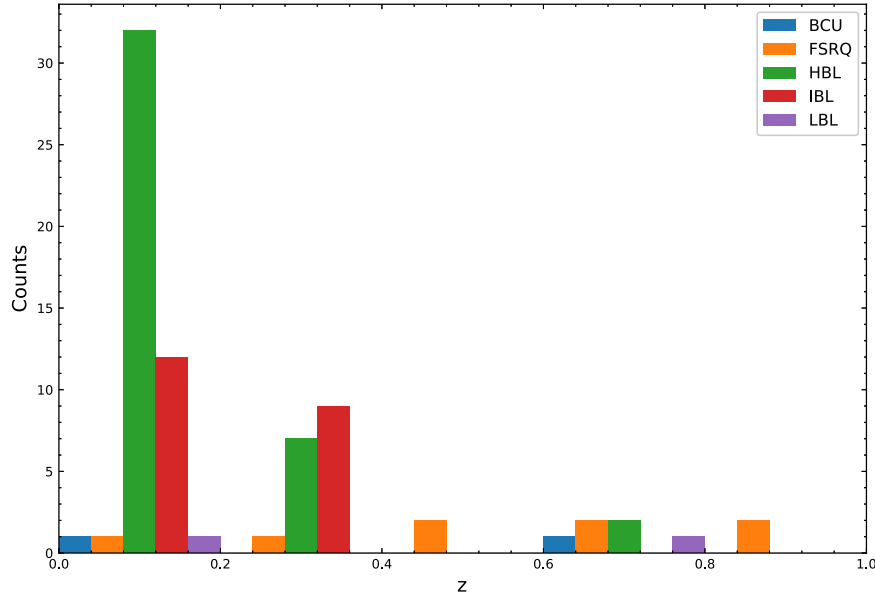


**Figure 1.** The redshift distribution of each type of blazar in the sample. The histogram is illustrated in five bins, which are  $0 \sim 0.2$ ,  $0.2 \sim 0.4$ ,  $0.4 \sim 0.6$ ,  $0.6 \sim 0.8$ , and  $0.8 \sim 1.0$ . The blue bar stands for BCU, the orange bar stands for FSRQ, the green bar stands for HBL, the red bar stands for IBL, and the violet bar stands for LBL.

the sources within  $5^\circ$  from the target, as well as sources within the ROI with a variable index  $\geq 72.44$  (Acero et al. 2015), were set as free parameters. All other parameters were fixed at their catalog values in 4FGL-DR3. We used the original spectral models in 4FGL-DR3 for the sources in the source model when performing a binned maximum likelihood analysis with `gtlike`. A simple power-law ( $dN/dE \propto E^{-\Gamma}$ , where  $\Gamma$  is the photon index) spectral type was used for each blazar when deriving its light curve. We checked through the likelihood analysis results assuming a power-law model and compared it with a log-parabola ( $dN/dE \propto (E/E_0)^{-\alpha-\beta \log(E/E_0)}$ , where  $\alpha$  and  $\beta$  are spectral parameters) for the samples in the source models, and found that a log-parabola is not significantly preferred over a power law for the samples, except for J0035.9+5950 and J0221.1+3556. Therefore, we changed the two sources' spectral parameters accordingly in Table 1. The comparison was conducted by calculating  $\sqrt{-2 \log(L_{\text{pl}}/L_{\text{logP}})}$ , where  $L_{\text{pl}}$  and  $L_{\text{logP}}$  are the maximum likelihood values obtained from a power law and a log-parabola, respectively (Abdo et al. 2013). In addition, the background galactic and extragalactic diffuse emission models were added to the source model using the spectral model file `gll_iem_v07.fits` and `iso_P8R3_SOURCE_V2_v1.txt`, respectively. The normalizations of the two diffuse emission components were set as free parameters in the analysis. We constructed light curves binned in 90 day time intervals by performing standard binned maximum likelihood analysis, calculated flux ( $F_\gamma$ ) and photon spectral index ( $\Gamma$ ) for the energy range of 1–300 GeV spectrum and listed them in columns (5) and (6) of Table 1.

### 3. Results

#### 3.1. Annual and Monthly Intensities at the GeV Band

Fermi-LAT has conducted observations at  $\gamma$ -ray energy bands over 15 yr by scanning the whole sky every 3 hr. We aim to provide detailed GeV spectral behaviors, study the GeV variability of the TeV blazars, and put constraints on the blazar emission model. We calculated the annual GeV fluxes and corresponding photon spectral indices for the 78 TeV blazars in

our sample and listed them in Table 2, in which the annual (360 day time interval) maximum, the minimum, and the mean fluxes and the corresponding photon spectral indices are given for the past 15 yr since the launch of Fermi (MJD 54683).

Moreover, according to the 90 day binned light curves we select a subsample of bright blazars. The selection criterion is that the source has at least one-third of data points that have maximum likelihood test statistic (TS) values larger than 75 (3 times the  $5\sigma$  detection significance); there are 41 blazars are selected and marked by “Y” for the bright flag in Table 2. We further constructed 30 day binned light curves for these 41 TeV blazars. The monthly binned light curves are shown in Figure 2, for which only the flux data points with the maximum likelihood TS values larger than 9 are plotted. To further investigate the spectral behavior of these 41 bright TeV blazars, we calculated the detailed monthly flux and corresponding photon spectral index and listed them in Tables 3 and 4. In these two tables, the MJD time represents the beginning of each bin. The TS values for each MJD time of each blazar are listed in parentheses. Note that in some periods, there may be situations where the spectral photon index is too large or too small, which requires simultaneous consideration of the TS value. Usually, we use data points with TS values larger than 9 in the analysis.

#### 3.2. GeV Luminosity and Spectral Photon Index

The  $\gamma$ -ray luminosity is calculated by

$$L_\gamma = 4\pi d_L^2 (1+z)^{(\Gamma-2)} F_\gamma, \quad (1)$$

where

$$d_L = \frac{c}{H_0} \int_1^{1+z} \frac{1}{\sqrt{\Omega_m x^3 + 1 - \Omega_m}} dx \quad (2)$$

is a luminosity distance (Komatsu et al. 2011) and  $(1+z)^{(\Gamma-2)}$  stands for a  $K$  correction. We calculated the  $\gamma$ -ray luminosity of the 74 blazars for which we have redshift information, using the energy flux derived from the binned likelihood analysis,

**Table 2**  
Annual GeV Fluxes and Photon Indices for the 78 TeV Blazars in Our Sample

Name	Bright	2008–2009	2009–2010	2010–2011	2011–2012	2012–2013	2013–2014	2014–2015	2022–2023	
$f_{\gamma}^{\max}$	J0013.9-1854	$7.2 \pm 3.5$	$5.5 \pm 3.5$	$12 \pm 4.7$	$5.6 \pm 3.4$	$8.7 \pm 4.1$	$3.9 \pm 3.4$	$5.7 \pm 3.2$	$5.2 \pm 11$	
$f_{\gamma}^{\min}$		$0.00082 \pm 1.1$	$1.2 \pm 1.2$	$0.0067 \pm 0.55$	$2 \pm 2.6$	$6.2e-05 \pm 0.00023$	$1.2 \pm 1.9$	$0.67 \pm 2.2$	$9.5e-05 \pm 0.15$	
$f_{\gamma}^{\text{mean}}$		3.3	2.4	4	3.6	3.3	2.5	3.4	1.7	
$\Gamma^{\max}$		$2.6 \pm 1$	$2.8 \pm 1.9$	$10 \pm 0.068$	$5.8 \pm 3.5$	$2.1 \pm 1.6e+02$	$10 \pm 1.3$	$3.3 \pm 3.2$	$4.2 \pm 11$	
$\Gamma^{\min}$		$1.7 \pm 0.55$	$0.78 \pm 0.66$	$2.6 \pm 0.59$	$2.5 \pm 1.2$	$1.4 \pm 0.6$	$1.1 \pm 0.6$	$1.4 \pm 0.34$	$1.3 \pm 7.5e+02$	
$\Gamma^{\text{mean}}$		2	1.8	5.4	4.3	1.8	3.9	2.3	2.8	
$f_{\gamma}^{\max}$	J0033.5-1921	Y	$50 \pm 13$	$79 \pm 17$	$87 \pm 19$	$69 \pm 17$	$49 \pm 16$	$54 \pm 17$	$62 \pm 16$	$34 \pm 11$
$f_{\gamma}^{\min}$			$10 \pm 6.6$	$11 \pm 8.3$	$9.9 \pm 7.4$	$11 \pm 8$	$7.5 \pm 7.4$	$16 \pm 8$	$12 \pm 12$	$22 \pm 11$
$f_{\gamma}^{\text{mean}}$			31	36	28	32	24	26	32	27
$\Gamma^{\max}$			$2.7 \pm 0.63$	$2.6 \pm 0.55$	$10 \pm 0.068$	$2.8 \pm 0.78$	$5.3 \pm 3.7$	$3.4 \pm 1.1$	$2.3 \pm 2.1$	$2.3 \pm 0.4$
$\Gamma^{\min}$			$1.5 \pm 0.29$	$1.5 \pm 0.24$	$0.9 \pm 0.35$	$1.5 \pm 0.25$	$1.5 \pm 0.29$	$0.77 \pm 0.63$	$1.3 \pm 0.39$	$1.1 \pm 0.23$
$\Gamma^{\text{mean}}$			2	2	2.4	1.8	2.5	2	1.7	1.8
$f_{\gamma}^{\max}$	J0035.9+5950	Y	$58 \pm 6.3$	$27 \pm 7.5$	$40 \pm 15$	$52 \pm 17$	$73 \pm 11$	$98 \pm 19$	$70 \pm 6.6$	$36 \pm 9.3$
$f_{\gamma}^{\min}$			$4.7 \pm 3.9$	$8.9 \pm 4.7$	$4.8 \pm 4.7$	$12 \pm 7$	$13 \pm 3$	$9 \pm 7.6$	$28 \pm 15$	$4.5 \pm 4.4$
$f_{\gamma}^{\text{mean}}$			26	16	27	24	31	54	53	15
$\Gamma^{\max}$			$5 \pm 0.001$	$5 \pm 0.73$	$3.7 \pm 0.0029$	$3.2 \pm 0.0054$	$2.7 \pm 0.19$	$2.2 \pm 0.34$	$2.7 \pm 0.053$	$2.9 \pm 0.0032$
$\Gamma^{\min}$			$0.15 \pm 0.12$	$0.14 \pm 0.12$	$0.82 \pm 0.024$	$0.65 \pm 0.25$	$0.32 \pm 0.014$	$0.32 \pm 0.15$	$0.56 \pm 0.049$	$0.92 \pm 0.14$
$\Gamma^{\text{mean}}$			2	2.2	2.1	1.8	1.4	1.4	1.7	1.9
$f_{\gamma}^{\max}$	J0112.1+2245	Y	$93 \pm 17$	$2.6e+02 \pm 29$	$2.4e+02 \pm 30$	$1.6e+02 \pm 24$	$66 \pm 17$	$1.1e+02 \pm 21$	$1.8e+02 \pm 31$	$1.6e+02 \pm 28$
$f_{\gamma}^{\min}$			$16 \pm 10$	$34 \pm 12$	$21 \pm 9.3$	$60 \pm 16$	$9.8 \pm 6.9$	$9.1 \pm 6$	$21 \pm 11$	$39 \pm 11$
$f_{\gamma}^{\text{mean}}$			56	88	77	$1.1e+02$	39	52	$1e+02$	80
$\Gamma^{\max}$			$4.5 \pm 1.7$	$2.6 \pm 0.41$	$3.8 \pm 1.1$	$2.9 \pm 0.38$	$6.7 \pm 2.9$	$3 \pm 1.1$	$3 \pm 0.76$	$2.6 \pm 0.29$
$\Gamma^{\min}$			$1.9 \pm 0.37$	$1.8 \pm 0.2$	$1.7 \pm 0.27$	$1.8 \pm 0.2$	$1.9 \pm 0.58$	$1.5 \pm 0.47$	$1.5 \pm 0.35$	$2 \pm 0.23$
$\Gamma^{\text{mean}}$			2.6	2.1	2.5	2.2	2.8	2.4	2.1	2.3
$f_{\gamma}^{\max}$	J0136.5+3906	Y	$78 \pm 18$	$66 \pm 15$	$1.2e+02 \pm 19$	$62 \pm 16$	$65 \pm 16$	$54 \pm 15$	$53 \pm 14$	$91 \pm 18$
$f_{\gamma}^{\min}$			$18 \pm 7.9$	$32 \pm 12$	$45 \pm 13$	$23 \pm 8.9$	$29 \pm 10$	$14 \pm 11$	$16 \pm 13$	$27 \pm 13$
$f_{\gamma}^{\text{mean}}$			42	48	65	47	41	37	35	46
$\Gamma^{\max}$			$2.1 \pm 0.3$	$2.2 \pm 0.36$	$2.2 \pm 0.31$	$2.4 \pm 0.38$	$2.2 \pm 0.39$	$2.1 \pm 0.28$	$2.2 \pm 0.97$	$2 \pm 0.28$
$\Gamma^{\min}$			$1.4 \pm 0.29$	$1.3 \pm 0.2$	$1.5 \pm 0.16$	$1.4 \pm 0.3$	$1.5 \pm 0.24$	$1.5 \pm 0.21$	$1.4 \pm 0.26$	$1.4 \pm 0.33$
$\Gamma^{\text{mean}}$			1.8	1.8	1.7	1.7	1.8	1.7	1.8	1.7

**Note.**  $f_{\gamma}$  is in units of  $10^{-10} \text{ ph} \cdot \text{cm}^{-2} \cdot \text{s}^{-1}$ , and only five items are presented.

(This table is available in its entirety in machine-readable form.)

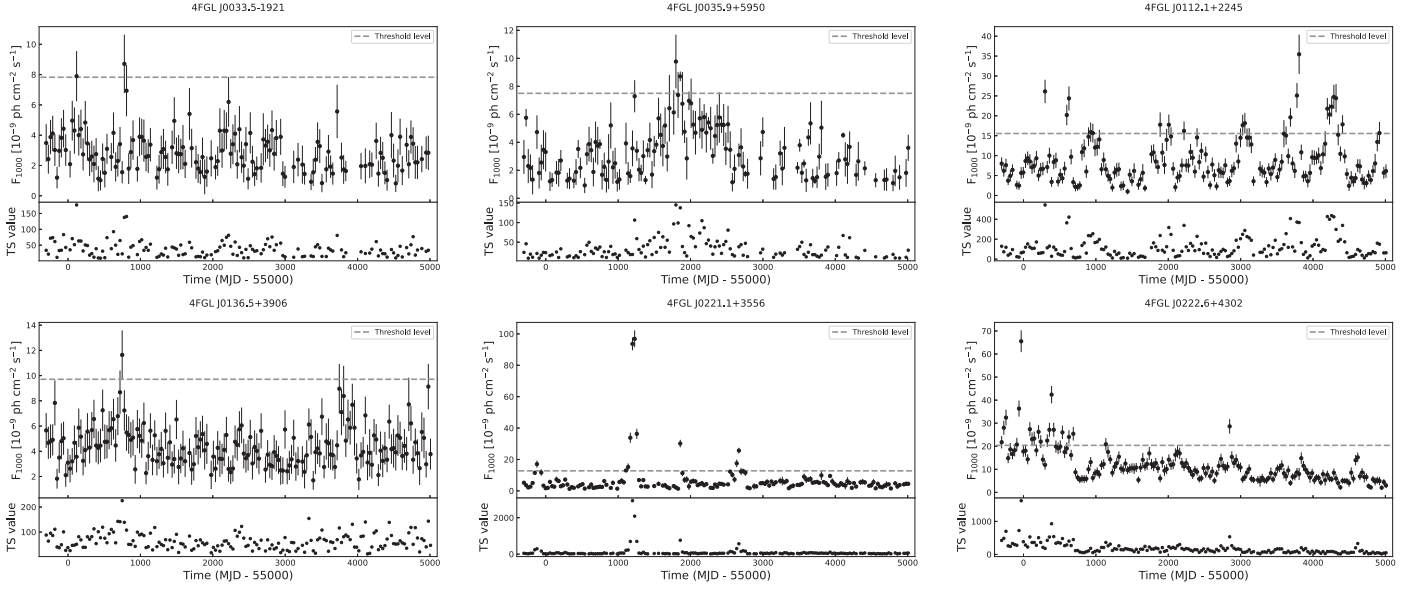


**Figure 2.** The monthly binned light curves for the 41 bright blazars in our sample. Only six items are presented here. (The complete figure set (41 images) is available.)

and studied the correlations between the GeV  $\gamma$ -ray luminosity and photon index shown in Figure 3.

It is found that FSRQs occupy the upper-right region, the IBLs occupy the middle region, and the high-energy peaked BL Lacs (HBLs) occupy the lower-left region of Figure 3. This result suggests that the TeV blazars show a decrease in the GeV  $\gamma$ -ray luminosity and photon spectral index with the increase in synchrotron peak frequency, and indicates a *blazar sequence* that was initially proposed by Fossati et al. (1998). In addition, we calculated the linear regressions between  $\Gamma$  and  $\log L_\gamma$  as

$$\Gamma = (-0.18 \pm 0.05) \log L_\gamma + (10.98 \pm 2.36)$$

with the correlation coefficient  $r = -0.84$  and the chance probability  $p = 0.01$  for FSRQs through a Pearson analysis:

$$\Gamma = (-0.03 \pm 0.03) \log L_\gamma + (3.16 \pm 1.19)$$

with  $r = -0.23$ ,  $p = 0.31$  for IBLs;

$$\Gamma = (-0.07 \pm 0.01) \log L_\gamma + (5.06 \pm 0.48)$$

with  $r = -0.74$ ,  $p = 2.60 \times 10^{-8}$  for the HBLs. The regression results are shown in Figure 3 and suggest a strong correlation between  $\Gamma$  and  $\log L_\gamma$  for the FSRQs and HBLs, while there is no correlation for IBLs. We also conducted statistics on the weighted Kendall's tau (Shieh 1998) and Spearman's coefficients. The  $r$  values obtained through the weighted Kendall's tau analysis were  $-0.74$ ,  $-0.60$ , and  $-0.28$  for FSRQs, HBLs, and IBLs respectively. The coefficient obtained using Spearman's statistics is  $r = -0.86$ ,  $p = 6.53 \times 10^{-3}$ ,  $r = -0.59$ ,  $p = 4.96 \times 10^{-5}$ , and  $r = -0.26$ ,  $p = 0.26$  for FSRQs, HBLs, and IBLs respectively. These results supported that of the Pearson's analysis mentioned above.

Ackermann et al. (2015) and Ajello et al. (2020) showed the LAT photon index versus the  $\gamma$ -ray luminosity for the different blazar subclasses of the whole sample in the Third LAT AGN Catalog (3LAC) and the Fourth LAT AGN Catalog (4LAC) blazars. The trend of softer spectra with higher luminosity reported in previous catalogs is also confirmed. However,

4LAC noted that the correlation between photon index and  $\gamma$ -ray luminosity is significant overall for blazars, but much weaker when the different classes are taken independently. While 3LAC  $\gamma$ -ray luminosity results were computed from the Fermi-LAT Four-Year Source Catalog (3FGL) energy flux between 100 MeV and 100 GeV. They also mentioned that due to the bias in the selection criteria for the 57 BL Lacs with both lower and upper limits on their redshifts or only upper limits, the HBLs with both limits were found to be more luminous on average than those with measured redshifts.

### 3.3. GeV Flux and Spectral Photon Index in Flares

We note that 28 of our teraelectronvolt blazar samples were reported in the Second Fermi All-sky Variability Analysis Catalog (2FAV; Abdollahi et al. 2017). The analysis of 2FAV was run in weekly time bins using the first 7.4 yr of Fermi data in two independent energy bands, 100–800 MeV and 0.8–300 GeV. We have checked these light curves to find the GeV outbursts/flares that meet the criterion, which is that a source shows flare flux more than 10 times larger than its flux in quiescent states and the significance compared to the quiescent light curves is more than  $5\sigma$  simultaneously. There are 14 sources that showed significant outbursts/flares at the GeV band during the Fermi campaign, and these sources are listed in Table 5. All of these significant flares have been reported in 2FAV, except for J1422.3+3223. The photon indices and fluxes of these 14 blazars with bright flares in the 1–300 GeV band are shown in Figure 4, for which only the flux data points with  $TS > 9$  were selected for the plot. The insets in Figure 4 display the photon index resulting from an analysis where photons were sorted in five bins in 5 day flux, plotted versus the 5 day flux. Fluxes and photon indices during their flaring states are listed in columns (4) and (5) of Table 5, respectively.

For these 14 blazars with bright flares, we constructed light curves in the 5 day bin in their flaring states. There are six blazars that showed a clear single sharp peak profile contained in the flare that meet the criterion, which is that its flare flux is

**Table 3**  
Monthly GeV Photon Fluxes of the 41 Bright TeV Blazars

MJD	J0033.5-1921	J0035.9+5950	J0112.1+2245	J0136.5+3906	J0221.1+3556	J0222.6+4302	J0303.4-2407
54683	$3.49\text{e}+01 \pm 1.24\text{e}-09$	$2.95\text{e}-09 \pm 1.21\text{e}-09$	$8.00\text{e}-09 \pm 1.56\text{e}-09$	$5.66\text{e}-09 \pm 1.38\text{e}-09$	$5.18\text{e}-09 \pm 8.65\text{e}-10$	$2.18\text{e}-08 \pm 2.68\text{e}-09$	$2.97\text{e}-09 \pm 1.01\text{e}-09$
54713	$2.42\text{e}-09 \pm 9.60\text{e}-10$	$5.75\text{e}-09 \pm 6.32\text{e}-10$	$6.19\text{e}-09 \pm 1.46\text{e}-09$	$4.67\text{e}-09 \pm 1.28\text{e}-09$	$3.57\text{e}-09 \pm 9.36\text{e}-10$	$2.80\text{e}-08 \pm 3.06\text{e}-09$	$3.40\text{e}-09 \pm 1.09\text{e}-09$
54743	$3.88\text{e}-09 \pm 1.13\text{e}-09$	$2.30\text{e}-09 \pm 1.22\text{e}-09$	$7.59\text{e}-09 \pm 1.64\text{e}-09$	$4.79\text{e}-09 \pm 1.33\text{e}-09$	$2.13\text{e}-09 \pm 1.03\text{e}-09$	$3.24\text{e}-08 \pm 3.43\text{e}-09$	$4.62\text{e}-09 \pm 1.31\text{e}-09$
54773	$4.11\text{e}-09 \pm 1.17\text{e}-09$	$2.17\text{e}-09 \pm 9.61\text{e}-10$	$3.71\text{e}-09 \pm 1.12\text{e}-09$	$4.91\text{e}-09 \pm 1.24\text{e}-09$	$2.68\text{e}-09 \pm 9.27\text{e}-10$	$1.48\text{e}-08 \pm 2.18\text{e}-09$	$2.11\text{e}-09 \pm 9.25\text{e}-10$
54803	$3.02\text{e}-09 \pm 1.05\text{e}-09$	$1.33\text{e}-09 \pm 1.05\text{e}-09$	$4.92\text{e}-09 \pm 1.40\text{e}-09$	$7.84\text{e}-09 \pm 1.79\text{e}-09$	$4.99\text{e}-09 \pm 1.24\text{e}-09$	$1.86\text{e}-08 \pm 2.78\text{e}-09$	$3.10\text{e}-09 \pm 1.09\text{e}-09$

**Note.**  $f_\gamma$  is in units of  $\text{ph} \cdot \text{cm}^{-2} \cdot \text{s}^{-1}$ .

(This table is available in its entirety in machine-readable form.)

**Table 4**  
Monthly GeV Photon Indices of the 41 Bright TeV Blazars

MJD	J0033.5-1921	J0035.9+5950	J0112.1+2245	J0136.5+3906	J0221.1+3556	J0222.6+4302	J0303.4-2407
54683	$2.06 \pm 0.34$ (33.87)	$1.48 \pm 0.39$ (23.96)	$2.29 \pm 0.24$ (129.66)	$1.81 \pm 0.21$ (87.97)	$3.15 \pm 0.03$ (44.27)	$1.89 \pm 0.11$ (422.97)	$1.99 \pm 0.34$ (40.08)
54713	$2.68 \pm 0.63$ (21.77)	$1.52 \pm 0.07$ (45.82)	$2.75 \pm 0.38$ (73.61)	$1.93 \pm 0.25$ (63.71)	$4.39 \pm 0.04$ (28.20)	$2.14 \pm 0.12$ (486.64)	$2.19 \pm 0.37$ (53.06)
54743	$1.71 \pm 0.23$ (72.02)	$2.05 \pm 0.29$ (9.12)	$2.13 \pm 0.23$ (119.35)	$1.46 \pm 0.20$ (95.25)	$3.88 \pm 0.03$ (17.48)	$1.77 \pm 0.09$ (699.83)	$2.06 \pm 0.29$ (65.38)
54773	$1.71 \pm 0.23$ (73.58)	$0.96 \pm 0.57$ (19.40)	$2.89 \pm 0.52$ (39.78)	$1.75 \pm 0.20$ (86.03)	$0.72 \pm 1.37$ (46.57)	$2.21 \pm 0.17$ (258.71)	$1.94 \pm 0.47$ (25.62)
54803	$1.46 \pm 0.24$ (61.40)	$1.03 \pm 0.06$ (11.54)	$2.49 \pm 0.39$ (53.79)	$1.90 \pm 0.21$ (111.16)	$2.43 \pm 0.09$ (50.73)	$2.38 \pm 0.20$ (242.92)	$1.75 \pm 0.29$ (47.64)

(This table is available in its entirety in machine-readable form.)

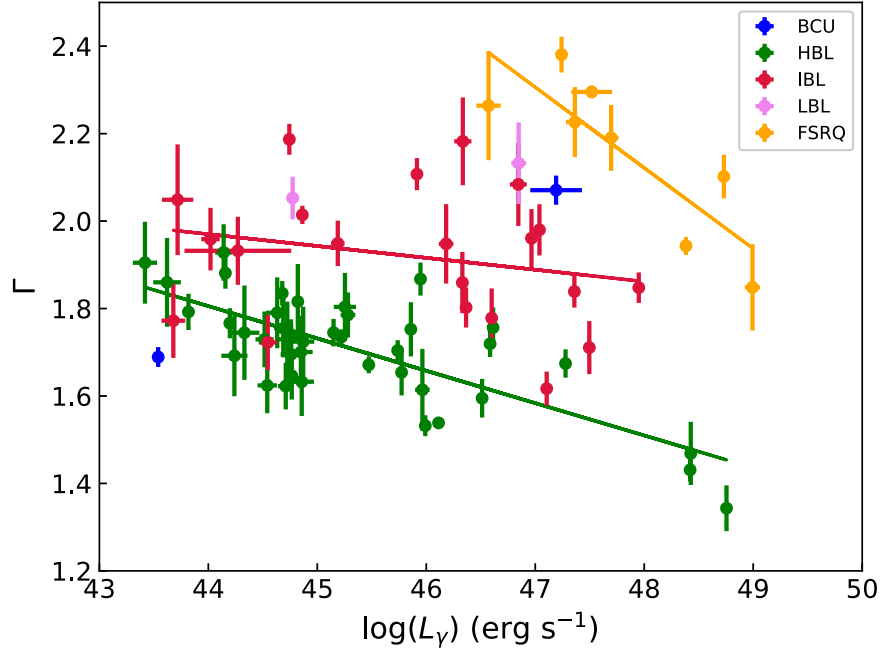


**Figure 3.** The correlation between 1 and 300 GeV photon indices and the luminosity of 74 blazars. The solid lines represent the fitting results of the linear regressions.

**Table 5**  
Fluxes, Photon Indices, Fitting Results for the Flaring Sharp Peaks, and Asymmetry Parameters of the Bright GeV Flares of 14 TeV Blazars

4FGL Name (1)	$z$ (2)	Class (3)	$f_\gamma$ ( $\text{ph} \cdot \text{cm}^{-2} \cdot \text{s}^{-1}$ ) (4)	$\Gamma$ (5)	$\alpha$ (6)	$T_r$ (day) (7)	$T_d$ (day) (8)	$k$ (9)
J0221.1+3556	0.944	FSRQ	$9.51\text{e-}08 \pm 3.05\text{e-}09$	$2.54 \pm 0.03$	...	...	...	...
J0303.4-2407	0.26	IBL	$5.15\text{e-}08 \pm 3.89\text{e-}09$	$1.97 \pm 0.08$	...	$0.33 \pm 1.43$	$6.26 \pm 0.91$	-0.90
J0739.2+0137	0.189	FSRQ	$3.78\text{e-}08 \pm 2.99\text{e-}09$	$2.55 \pm 0.12$	4.20	$0.26 \pm 1.74$	$3.36 \pm 1.47$	-0.86
J0904.9-5734	0.695	BCU	$2.09\text{e-}07 \pm 5.22\text{e-}09$	$2.19 \pm 0.02$	2.76	...	...	...
J0958.7+6534	0.367	IBL	$7.66\text{e-}08 \pm 4.58\text{e-}09$	$2.16 \pm 0.07$	2.64	$6.72 \pm 1.45$	$12.32 \pm 1.97$	-0.29
J1159.5+2914	0.729	FSRQ	$1.74\text{e-}07 \pm 2.38\text{e-}08$	$2.20 \pm 0.05$	2.80	...	...	...
J1224.9+2122	0.435	FSRQ	$1.63\text{e-}07 \pm 1.18\text{e-}08$	$2.39 \pm 0.06$	3.56	...	...	...
J1230.2+2517	0.135	IBL	$3.08\text{e-}08 \pm 2.64\text{e-}09$	$2.06 \pm 0.09$	2.24	...	...	...
J1256.1-0547	0.536	FSRQ	$3.52\text{e-}07 \pm 8.72\text{e-}09$	$2.44 \pm 0.04$	3.76	...	...	...
J1422.3+3223	0.682	FSRQ	$1.25\text{e-}07 \pm 1.41\text{e-}08$	$2.29 \pm 0.05$	3.16	$9.15 \pm 0.79$	$5.90 \pm 0.44$	0.22
J1443.9+2501	0.939	FSRQ	$4.04\text{e-}08 \pm 1.95\text{e-}09$	$2.23 \pm 0.06$	2.92	...	...	...
J1512.8-0906	0.36	FSRQ	$1.78\text{e-}07 \pm 4.90\text{e-}09$	$2.49 \pm 0.04$	...	$1.67 \pm 0.43$	$1.13 \pm 2.99$	0.19
J1751.5+0938	0.322	LBL	$1.12\text{e-}07 \pm 5.62\text{e-}09$	$2.27 \pm 0.06$	3.08	$5.20 \pm 1.18$	$1.96 \pm 0.59$	0.45
J2202.7+4216	0.069	IBL	$2.34\text{e-}07 \pm 4.17\text{e-}09$	$2.10 \pm 0.02$	2.40	...	...	...

**Note.** Column (1): 4FGL name; column (2): the redshift; column (3): the classification determined based on the synchrotron peak frequency; column (4): fluxes during flaring states; column (5): photon indices during flaring states; column (6): the electron spectra index in Section 4.3; column (7): the rise-time fitting results for the flaring sharp peaks in units of days; column (8): the decay-time fitting results for the flaring sharp peaks in units of day; column (9): the parameter of the flare asymmetry.

(This table is available in machine-readable form.)

more than 12 times larger than its flux in quiescence and the significance compared to the quiescent states is more than  $4\sigma$  simultaneously. We also searched intraday flares and only found 4FGL J1256.1-0547 (3C 279) had minute-scale variability in 2018, and this result has been reported in our previous work (Wang et al. 2022a). We determined the properties of the six single sharp peak cases by fitting their profiles with a formula given by

$$F(t) = F_c + F_0(e^{(t-t_0)/T_r} + e^{(t-t_0)/T_d})^{-1}, \quad (3)$$

where  $F_c$  and  $F_0$  are the constant flux and height of a peak, respectively,  $t_0$  is the flux peak time, and  $T_r$  and  $T_d$  are used to measure the rise and decay time in units of days. We show the flare profiles in Figure 5 for flares with a single sharp peak, and the distribution of rise and decay time in Figure 6.

We calculate the parameter of the flare asymmetry following Chatterjee et al. (2012) as

$$k = \frac{T_r - T_d}{T_r + T_d}. \quad (4)$$

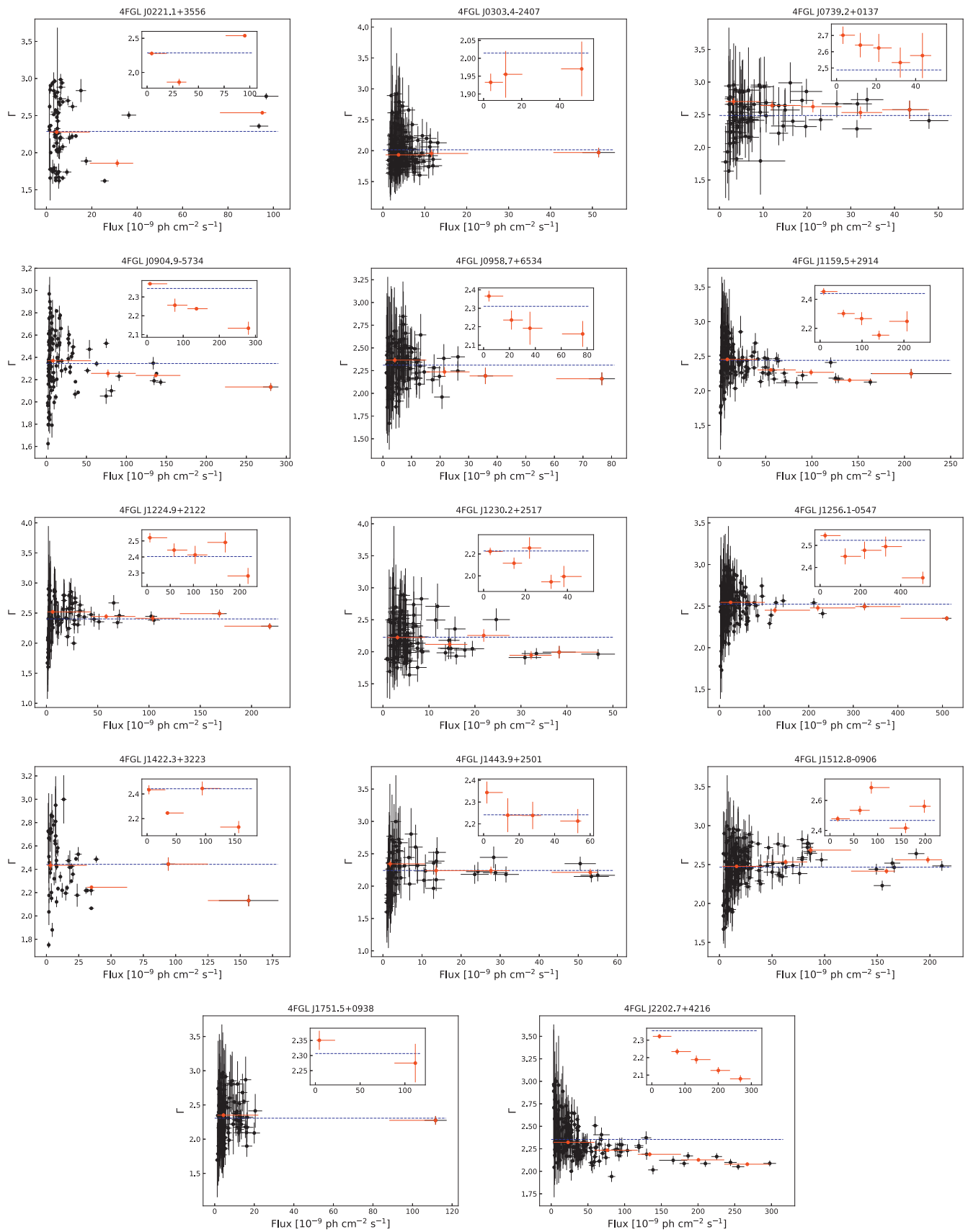


**Figure 4.** 1–300 GeV photon indices and fluxes of blazars with bright flares. Only data points with  $TS > 9$  are plotted. The blue dashed horizontal lines indicate the average photon indices of those data. The insets show the photon index resulting from an analysis where photons were sorted in five bins using 5 day fluxes plotted vs. the 5 day flux (red points).

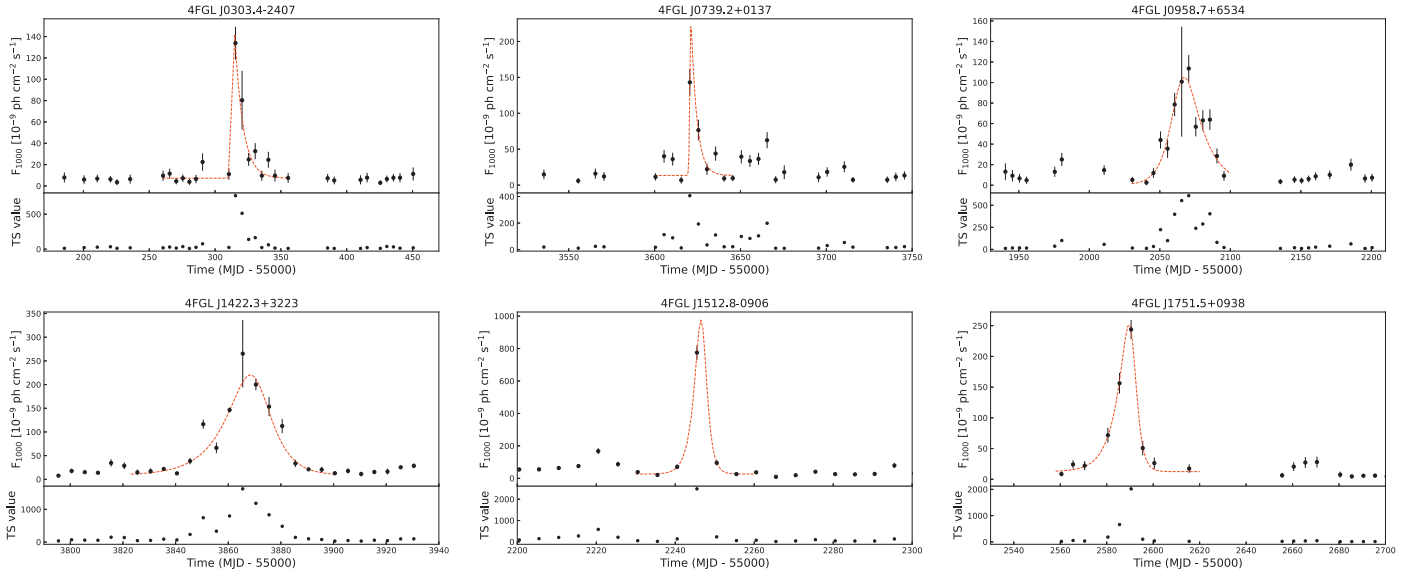


**Figure 5.** Flare profiles for six TeV blazars with a single sharp peak in their 5 day binned light curves; an analytic function (dashed red curve) was used to fit the profile.

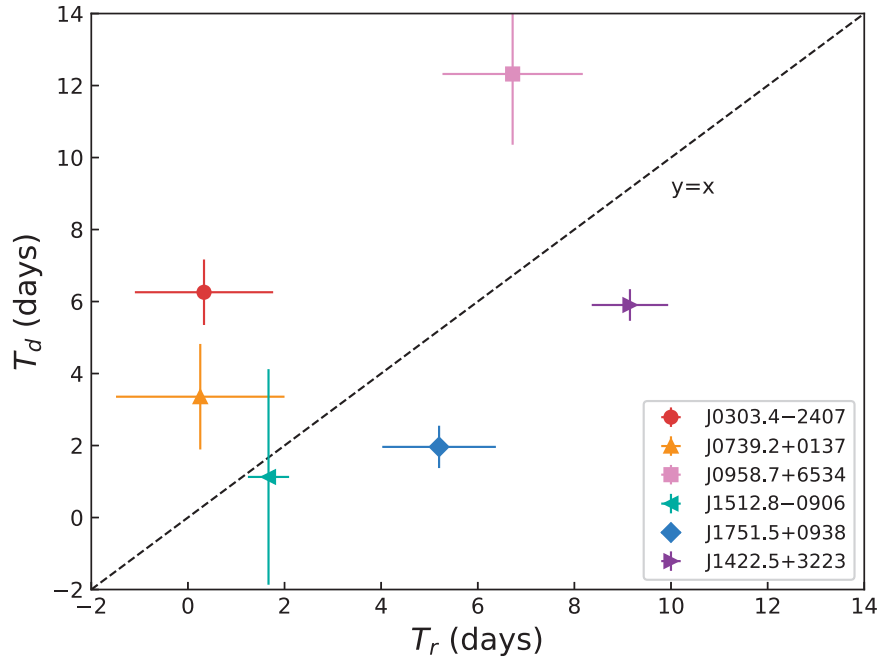


**Figure 6.** Distribution of rise and decay time for the six sharp peak flare profiles fitted to the data.

The results are listed in column (9) of Table 5, while  $k < 0$  indicates a fast rise exponential decay (FRED) type flare. Approximately,  $k < -0.3$  indicates faster rise than decay,  $k > 0.3$  indicates faster decay than rise, while  $-0.3 < k < 0.3$  indicates a symmetric profile,  $k = 0$  for exactly symmetric flares. Among the six sharp peak flares, 4FGL J0303.4-2407 and 4FGL J0739.2+0137 show FRED behavior, 4FGL J1751.5+0938 shows the opposite, and the other three show symmetric profiles. Chatterjee et al. (2012) showed the distribution of the flare asymmetry parameter ( $k$ ) for the optical and  $\gamma$ -ray flares with a sample of six blazars, which indicated that most of the flare profiles are symmetric at both wave

bands. Abdo et al. (2010c) provided a systematic analysis of a larger sample of 106 objects by using the first 11 months of data from the Fermi survey and found only four sources with markedly asymmetric flares.

## 4. Discussion

### 4.1. Connection with the TeV Band

We have checked the coincidence between Fermi-LAT GeV detections and TeV detections of the sample. There are 22 sources in Table 1 that have detected TeV emission during the flaring states observed by Fermi-LAT, and 56 sources were in

the low state. J0509.4+0542 (TXS 0506+056) was detected at VHE by MAGIC and VERITAS (Abeysekara et al. 2018; Ansoldi et al. 2018; Acciari et al. 2022). It was in an active flaring state around the arrival of the high-energy neutrino IceCube-170922A (IceCube Collaboration et al. 2018b). Garrappa et al. (2019) found another blazar GB6 J1040+0617, in spatial coincidence with a neutrino in this sample and a chance probability of 30% after trial correction, indicating the source of this neutrino remains unknown. J1015.0+4926 was detected in a flaring state at VHE by MAGIC during 2014 February–March (Ahnen et al. 2016), and the Fermi-LAT observation was coincident with the TeV detection, and the GeV flux reached a level of 6.5 times higher than its low state. J1058.6+2817, Fermi-LAT, and MAGIC successively reported their flaring activity during 2021 March–April (Angioni 2021; Blanch 2021). J1217.9+3007's multi-wavelength observations with VERITAS and Fermi-LAT showed a well-connected high flux state in 2014 February (Abeysekara et al. 2017a). For J1728.3+5013, Archambault et al. (2015) reported the first detection of  $\gamma$ -ray flaring activity at VHE from this blazar; the flaring flux is about five times higher than its low state. Fermi-LAT detected this source with a mild flare and it observed a photon of energy of more than 300 GeV as reported in MAGIC Collaboration et al. (2020a). VERITAS detected VHE emission from J1813.5+3144 with flux similar to that reported by MAGIC (Benbow & VERITAS Collaboration 2022), during the active state observed by Fermi-LAT in 2020. J2000.0+6508 was reported to show flaring activity during 2016 June–July by Fermi-LAT and MAGIC (MAGIC Collaboration et al. 2020b). J2001.2+4353 showed a significant TeV detection on 2010 July 16, which was reported in Aleksić et al. (2014a), during the flaring activity observed by Fermi-LAT. J2243.9+2021 was also active in high energy during the time of VHE detection with the flux larger than the 4 yr averaged flux reported in 3FGL (Abeysekara et al. 2017b).

As for the 14 blazars that have bright flares, their flaring LAT states are all coincident with the TeV detections, except for J2202.7+4216. The detailed results are as follows:

1. J0221.1+3556, which was detected by MAGIC in 2014 July, was in its minor-flare state in Fermi-LAT observations, while its major-flare state was in 2012 September. The TeV detection was during the expected delayed component of the Fermi-LAT flare (Ahnen et al. 2016).
2. J0303.4-2407 was detected in a high state defined lasting from MJD 55312 (2010 April 26) to MJD 55323 (2010 May 5) reported by the H. E. S. S. Collaboration et al. (2013), which is also coincident with our result. However, the flaring TeV state in 2011 November was during the low state observed by Fermi-LAT.
3. J0739.2+0137: Its H. E. S. S. observation was triggered based on the detection of a Fermi-LAT flare, resulting in the detection of VHE  $\gamma$ -ray emission during the night of 2015 February 19. Therefore its flaring TeV state was coincident with the flaring Fermi-LAT state (H. E. S. S. Collaboration et al. 2020).
4. J0904.9-5734: H. E. S. S. observed a significant detection of VHE emission on 2020 April 13 (Wagner 2020), which is during the flaring state MJD 58931–58970 observed by Fermi-LAT.
5. J0958.7+6534 was detected in VHE  $\gamma$ -ray emission by MAGIC Collaboration et al. (2018) during the time period of 2015 February, 13–14, or MJD 57067. While Fermi-

LAT detected a 51 GeV photon from a very close position ( $0^{\circ}013$ ) to J0958.7+6534 on MJD 57066.98, indicating the coincidence with the MAGIC VHE detection (Tanaka et al. 2016).

6. J1159.5+2914: its time evolution of flux detected by Fermi-LAT was similar to the VHE light curve in its flaring states of 2017 and 2021 (Hirako et al. 2018; Adams et al. 2022).
7. J1224.9+2122: MAGIC detected its VHE emission around MJD 55364.9 (2010 June), this coincided with the flaring state at GeV energies (Hayes et al. 2011).
8. J1230.2+2517: Acharyya et al. (2023) reported follow-up multiwavelength observations of the discovery of VHE emission with VERITAS, showing the flaring states in high energy and VHE are coincident.
9. J1256.1-0547 (3C 279) has been extensively studied for its variability properties. For its GeV flare in 2015, the H. E. S. S. observation led to a clear detection during the end of the Fermi-LAT flaring state (Pittori et al. 2018; H. E. S. S. Collaboration et al. 2019). For its GeV flare in 2018, intense VHE flares were observed over multiple days after the end of the high-energy flares (Emery et al. 2019).
10. J1422.3+3223 was detected by MAGIC during its high state observed by Fermi-LAT, indicating the coincidence between the TeV detection and the flaring LAT state (MAGIC Collaboration et al. 2021).
11. J1443.9+2501 was reported by the VHE detection in the flaring state observed by Fermi-LAT (Abeysekara et al. 2015; Ahnen et al. 2015).
12. J1751.5+0938: H. E. S. S. detected an increase in flaring flux in 2016 (Schüssler et al. 2017), which is consistent with the flaring state observed by Fermi-LAT.
13. J1512.8-0906: the AGILE results of its flare in 2009 reported in D'Ammando et al. (2011) are in agreement with the Fermi-LAT results presented in Abdo et al. (2010b). For the subsequent flares in 2012 and 2015, the high-energy  $\gamma$ -ray light curve showed a mild flux variation compared to the strong flare at VHE energies (Zacharias et al. 2019; H. E. S. S. Collaboration et al. 2021).

## 4.2. Variability Analysis

### 4.2.1. Fractional Variability and Flare Profile

Variability is one of the main characteristics of blazars that have been studied in multi-bands (Urry 1996; Dermer 1999; Fan 1999; Singh & Meintjes 2020; Webb et al. 2021; Otero-Santos et al. 2022; Yuan et al. 2022). Abdo et al. (2010c) suggested that more than 50% of Fermi-detected bright blazars are found to be variable with high significance, and FSRQs and LBLs show higher variation amplitudes than the other blazars. We quantified the variability utilizing the fractional variability parameter  $F_{\text{var}}$ ;  $F_{\text{var}}$  can be described as (Vaughan et al. 2003)

$$F_{\text{var}} = \sqrt{\frac{S^2 - \langle \sigma_{\text{err}}^2 \rangle}{\langle F_{\gamma} \rangle^2}}, \quad (5)$$

where  $S^2$  is the variance of the flux,  $\langle \sigma_{\text{err}}^2 \rangle$  is the mean square value of uncertainties, and  $\langle F_{\gamma} \rangle$  is the mean photon flux. Negative values of  $F_{\text{var}}$  indicate very small or absent variability and/or slightly overestimated errors. We derived the mean

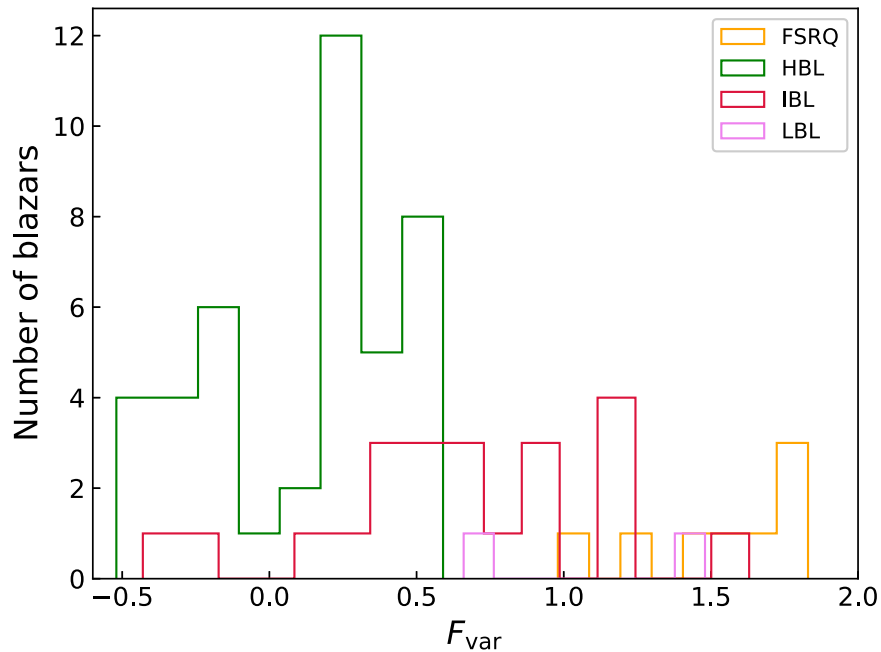


Figure 7. Distribution of the fractional variability  $F_{\text{var}}$  for the light curves of FSRQs, HBLs, IBLs, and LBLs.

values of  $F_{\text{var}}$  are  $1.54 \pm 0.02$ ,  $0.12 \pm 0.15$ ,  $0.65 \pm 0.06$ , and  $1.07 \pm 0.04$  for the FSRQs, HBLs, IBLs, and LBLs, respectively. The resulting values indicate that the flux of the FSRQs showed significantly stronger variability than that of the BL Lacs. As the synchrotron peak frequency decreases, the  $F_{\text{var}}$  value generally becomes larger. Here we presented a histogram of  $F_{\text{var}}$  values for the FSRQs, HBLs, IBLs, and LBLs in Figure 7. Bhatta & Dhital (2020) presented an analysis of a sample of 20 powerful blazars (12 BL Lacs and eight FSRQs) with 10 yr Fermi-LAT data, they obtained that the mean  $F_{\text{var}}$  value of BL Lacs is 0.58 and that of the FSRQs is 0.96. The results show that in general FSRQs are more variable than BL Lac sources in their sample, which is compatible with ours. Similar future studies involving larger samples should be carried out for a stronger conclusion. For the individual source, our result of S5 0716+714 is consistent with that reported in Bhatta et al. (2016), and the  $F_{\text{var}}$  values are 0.65, 0.57, 0.58, and 0.53 for the *BVRI* filters versus our 0.59.

Besides, we found 14 TeV blazars (eight FSRQs, one LBL, four IBLs, and one BCU) with outbursts/flares, and six out of the 14 flares showed sharp peak profiles in flares. Based on the sharp peak profiles, we notice 4FGL J0303.4-2407 and 4FGL J0739.2+0137 show fast-rising and slowly decaying subflares. This asymmetry can be related to the particle acceleration mechanism in the jet, a fast rise could result from an effective particle acceleration at the shock front and slow decay may be interpreted as the weakening of the shock (Sokolov et al. 2004; Tolamatti et al. 2022) or from the injection of energetic particles on a shorter timescale than the cooling process timescales (Acharyya et al. 2021). 4FGL J1751.5+0938 shows a slowly rising and fast-decaying subflare, which may be associated with an efficient cooling process.

#### 4.2.2. Flux Distributions

The analysis of flux distribution helps us determine whether the variability is caused by multiplicative or additive

mechanisms. Evidence for log-normality in blazars in  $\gamma$ -rays on different timescales has been reported for different sources (e.g., Kushwaha et al. 2017; Sinha et al. 2017; Bhatta & Dhital 2020). Similarly, the log-normal flux distribution of blazars was seen in 3LAC (Ackermann et al. 2015)). Shah et al. (2018) studied the flux distribution features of the selected 38 brightest Fermi blazars using the data collected during more than 8 yr and found that the flux distribution for 35 blazars supports a log-normal distribution, implying a multiplicative perturbation linked with the emission process. Using a large sample of 1414 variable blazars from the Fermi-LAT LCR catalog, Wang et al. (2023) thoroughly investigated the  $\gamma$ -ray flux distribution and statistical properties, and compared the flux distributions with normal and log-normal distributions. Their results showed that the probability of not rejecting the log-normal is 42.05%. We constructed histograms of the observed LAT GeV flux and fitted them to two different probability density functions (PDFs), a normal distribution and a log-normal distribution, and compared them with the results of  $\chi^2$ . To ensure sufficient data points for fitting the flux distribution, we selected the 41 bright blazars mentioned in Section 3.1. According to the  $\chi^2$  values from the fit, our results show that all of the bright blazars support a log-normal distribution rather than a normal distribution, which is also consistent with the results of previous studies. As there was consistency between the TeV detection and LAT observation discussed in Section 4.1, the TeV detections correspond to the outlier periods of the flux distribution. The parameters of the considered two distribution fitting results and the source flux histograms are shown in Table 6 and Figure 8; only some items are presented here.

#### 4.2.3. Flare Duty Cycle

The flaring state lasts only a fraction of the observation. Here we define the flaring state when any of the light curve's flux points exceeds a certain threshold following the method in

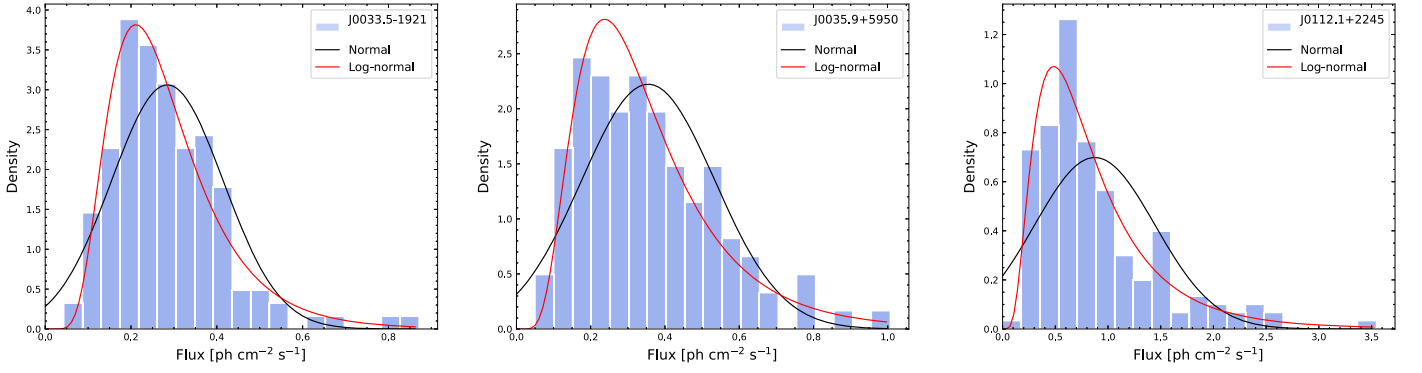


**Figure 8.** Flux distribution of the bright blazars in our sample in the GeV band. The black and red curves correspond to normal and log-normal fits, respectively. Only three items are presented here.

(The complete figure set (41 images) is available.)

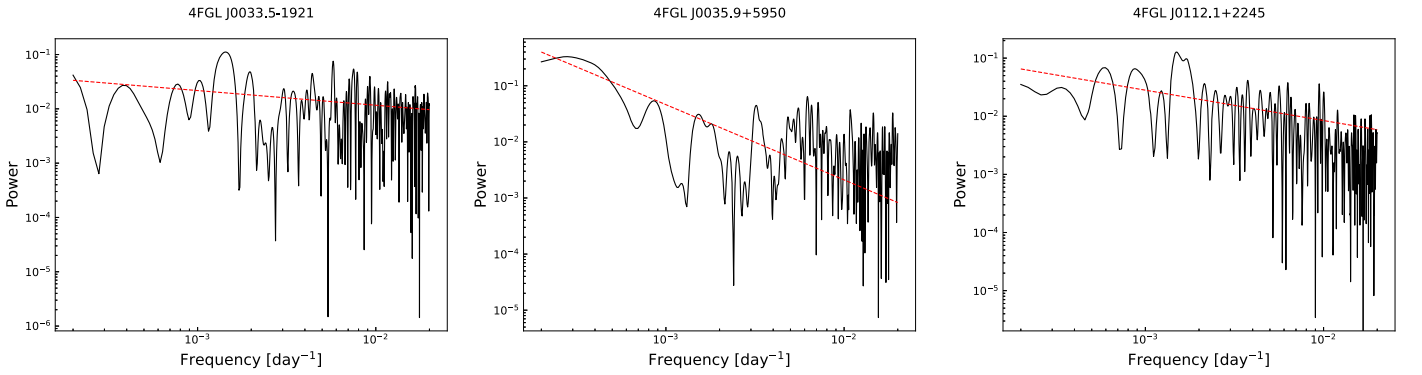


**Figure 9.** PSD fits with a power law for the LSPs of the bright blazars. The black curve indicates the raw LSP, and the red dashed line indicates the best fit. Only three items are presented here.

(The complete figure set (41 images) is available.)

**Table 6**  
Parameters of Normal and Log-normal Distribution Fitting for the  $\gamma$ -Ray Flux Distribution of the Fermi-LAT Sources

Name	Normal Fit			Log-normal Fit			$\beta_{\text{slope}}$
	Mean	$\sigma$	$\chi^2$	Mean	$\sigma$	$\chi^2$	
J0033.5-1921	0.28	0.13	2.19	-1.35	0.45	1.12	$0.27 \pm 0.03$
J0035.9+5950	0.35	0.18	2.05	-1.17	0.52	1.16	$1.34 \pm 0.03$
J0112.1+2245	0.87	0.57	1.07	-0.33	0.63	0.31	$0.52 \pm 0.02$
J0136.5+3906	0.44	0.16	1.35	-0.87	0.35	0.42	$0.58 \pm 0.02$
J0221.1+3556	0.66	1.11	0.93	-0.80	0.71	0.09	$0.57 \pm 0.02$
J0222.6+4302	1.19	0.79	0.48	-0.01	0.58	0.16	$0.91 \pm 0.02$
J0303.4-2407	0.48	0.45	0.68	-0.93	0.57	0.09	$0.25 \pm 0.02$

(This table is available in its entirety in machine-readable form.)

Yoshida et al. (2023),  $f_{\gamma}^{\text{th}}$ , which is given by

$$f_{\gamma}^{\text{th}} = f_{\gamma}^q + s \langle f_{\gamma}^{\text{err}} \rangle, \quad (6)$$

where  $f_{\gamma}^q$  is the quiescent level of  $\gamma$ -ray fluxes,  $\langle f_{\gamma}^{\text{err}} \rangle$  is the average uncertainty of the  $\gamma$ -ray fluxes, and  $s$  denotes the significance above the quiescent level in standard deviation units of  $\sigma$ . We use  $s = 6$  in this work, and the flaring threshold levels are plotted with dashed gray lines in Figure 2. From the light curves, we calculated the flare duty cycle (i.e., fraction of time spent in flaring states) for each flare. The flare duty cycle

is defined as

$$f_{\text{fl}} = \frac{1}{T_{\text{tot}}} \int_{f_{\gamma}^{\text{th}}} df_{\gamma} \frac{dT}{df_{\gamma}}, \quad (7)$$

where  $T_{\text{tot}}$  is the total observation time,  $f_{\gamma}$  is the  $\gamma$ -ray photon flux, and  $T$  is the time spent at the respective flux level. We find that our duty cycle results of the monthly binned light curves show values ranging from 0.0–0.36, and there is no evidence to show that the duty cycle is related to the TeV detection. Based on monthly binned light curves of the Fermi-LAT 2-Year Source Catalog (2FGL), Ackermann et al. (2011) showed that

bright blazars have flare duty cycles of about 0.05–0.10. In Table 2 in Abdollahi et al. (2017), the number of weekly binned flares detected for each source using the first 387 weeks of Fermi observations was presented, and the flare duty cycles appeared to suppress less than  $\sim 0.2$ . Yoshida et al. (2023) analyzed 145 gamma-ray bright blazars among the 4FGL catalog, and their results showed much broader distributions of flare duty cycles from the weekly binned light curves, ranging from 0.0–0.6. Our results of flare duty cycle values are similar to those of previous studies. Due to the vast majority of our results being in the range of 0.0–0.2, except for three sources with higher duty cycles (0.36 for J0721.9+7120, 0.26 for J1104.4+3812, and 0.26 for J2202.7+4216.)

#### 4.2.4. Power Spectral Densities

Power spectral density (PSD) is a mathematical function that characterizes the shape of a source periodogram. Similarly, in order to ensure the quality of the analysis, we analyzed the periodograms of the monthly binned  $\gamma$ -ray light curves of the 41 bright blazars applying a Lomb–Scargle periodogram (LSP; Lomb 1976; Scargle 1982). For frequency selection of the LSP analysis, the lower limit for the sampled frequencies, which corresponds to the length of the time series, is  $f_{\min} = 1/(t_{\max} - t_{\min})$ . Eyer & Bartholdi (1999) proposed a meaningful method to assess the Nyquist frequency that would be the upper limit of frequency,  $f_{\max}$ . The approach for selecting the frequency grid is to make each peak in the periodogram sampled as  $n_0 = 5$ –10 times (VanderPlas 2018). Then the total number of sampling frequencies would be  $N = n_0 \frac{f_{\max}}{f_{\min}}$ , and here we employ  $n_0 = 10$ . It is found that the periodograms are consistent with a power-law form of  $P(\nu) \propto \nu^{-\beta}$  with the slope index (spectral power index  $\beta$ ) ranging between 0.22 and 1.98. The mean PSD slope index of the sources is 0.74 with a standard deviation of 0.41. We listed the slope index results in Table 6, and the plots of the PSD are displayed in Figure 9.

Abdo et al. (2010c) conducted an analysis of the first 11 months of the LAT Bright AGN sample (LBAS), and revealed that the average  $\beta$  values of the brightest 22 FSRQs and the six brightest BL Lacs are 1.5 and 1.7, respectively. Ackermann et al. (2011) used 24 months of data and found that the  $\beta$  value is  $\sim 1.15 \pm 0.10$ , which is somewhat flatter than the results deduced from the LBAS sample. Tarnopolski et al. (2020) presented a comprehensive analysis of the Fermi-LAT 10 yr long light-curve modeling of 11 selected blazars by employing various methods. They found that the power-law slope index  $\beta$  calculated from the Fourier and LSP modeling mostly falls in the range of  $1 \lesssim \beta \lesssim 2$ . Our results for PKS 1510-089, PKS 2155-304, and Mrk 421 are consistent with the results in Sobolewska et al. (2014). They analyzed the  $\gamma$ -ray variability of 13 blazars with a linear superposition of Ornstein–Uhlenbeck processes, for which they found slopes to mostly be  $\beta \lesssim 1$ . Prokhorov & Moraghan (2017) obtained  $\beta = 0.67$  for PKS 2155-304, while we obtained  $\beta = 0.65 \pm 0.03$ . Also, our result for 3C 279 is similar to the PSD slopes found by Meyer et al. (2019). Chatterjee et al. (2012) found that the average slope of the PSD in the  $R$  band of six blazars is similar to that found by the Fermi team. Our result was in agreement for PKS 1510–089, but they obtained clearly steeper power-law fits than we did (2.3, 2.2 for 3C 279 and

PKS 2155–304 versus our 0.75, 0.65). Compared to these recent results of selecting the several brightest sources, our PSD result at the GeV band is slightly flatter and has a larger range. The discrepancies can be caused by the difference in the analysis methods, different binning schemes, sampling interval, and total duration of the observation of the analyzed light curves or methods of their generation between the works.

#### 4.2.5. Periodic Behaviors

The periodogram of the light curves can be characterized by a single power-law PSD. However, if we closely observe the structures of the periodogram, we may occasionally find peaks at certain frequencies, indicating the possible presence of (quasi)periodic signals in the observations. The periodic oscillation in the  $\gamma$ -ray band of blazar PG 1553+113 was reported by Ackermann et al. (2015c); this source is also contained in our sample and its light curve at the GeV band shows a clear periodicity, and has been explained in mechanisms invoking a supermassive binary black hole system (Cavaliere et al. 2017; Sobacchi et al. 2017). Several studies have systematically searched  $\gamma$ -ray quasiperiodic oscillations (QPOs) based on 3FGL (e.g., Prokhorov & Moraghan 2017; Peñil et al. 2020). Peñil et al. (2022) searched for periodicity in a sample of 24 blazars by using 12 well-established methods applied to Fermi 12 yr data, and found six out of the 24 sources showed light-curve periodicity with a global significance greater than  $3\sigma$ . Among our samples, some showed QPO characteristics in their  $\gamma$ -ray light curves. 12 blazars have been reported to have  $\gamma$ -ray QPOs according to Table 2 in Wang et al. (2022b), while nearly 30 blazars have been reported to show possible QPOs with high significance based on Fermi-LAT data so far. We note that various analysis methods can be affected by several caveats or effects that may have an impact when analyzing time series, and lead to the overestimation of signal significance. The caveats remind us of the complexity of the QPO analysis in AGNs, and the importance of correction of trials when computing probabilities. Otero-Santos et al. (2023) and Ren et al. (2023) have provided a detailed discussion of some of the caveats.

#### 4.3. Spectral Behavior

Variability is one of the main characteristics of blazars; the variability timescale spans from years to hours and even to minutes. The variability of flux is always accompanied by the variation of spectra. The correlation between the spectral index and flux has been investigated for individual sources and also for large samples (Fiorucci et al. 2004; Gu et al. 2006; Dai et al. 2009; Bonning et al. 2012; Raiteri et al. 2017; Yuan et al. 2017; Meng et al. 2018; Safna et al. 2020; Xiong et al. 2020). In general, this correlation was mainly discussed at the optical band and demonstrates *bluer-when-brighter* (BWB) behavior for BL Lacs, and shows *redder-when-brighter* (RWB) behavior for FSRQs, except in some special cases, e.g., 14 out of 29 Sloan Digital Sky Survey FSRQs show a BWB trend (Gu & Ai 2011), two out of 40 Fermi FSRQs exhibit a BWB trend and seven out of 13 BL Lacs exhibit an RWB trend (Zhang et al. 2022). Various models have been proposed to explain blazar optical spectral behavior, such as the shock-in-jet model (Rani et al. 2010), two-component (one variable + one stable) or one synchrotron model (Fiorucci et al. 2004), the energy injection model (Spada et al. 2001; Zhang et al. 2002), and also the

varying of the beaming effect (Larionov et al. 2010). Recently, Zhang et al. (2022) suggested a universal two-component model to interpret these two spectral behaviors, in which the observed optical emission of blazars consists of a stable or less variable thermal emission component ( $F_{\text{ther}}$ ) primarily coming from the accretion disk, and a highly variable nonthermal emission component ( $F_{\text{syn}}$ ) coming from the jet. The stronger the thermal emission component is, the bluer the color is, and the weaker the thermal emission is, the redder the color is.

However, the spectral behavior at higher energy bands seems monochrome. We found a universal BWB trend at the  $\gamma$ -ray band for the TeV blazars in our sample, especially the LBLs and FSRQs showing strong anticorrelation between the photon index and the GeV  $\gamma$ -ray luminosity. For the individual sources, Hayashida et al. (2012) performed a broadband study of the 3C 279 flare and found a BWB trend at the X-ray band and  $\gamma$ -ray bands. And this BWB trend was found again at the X-ray band for the same source during a phase of increased activity from 2013 December to 2014 April (Hayashida et al. 2015). Moreover, Aleksić et al. (2014b) made multifrequency observations of PKS 1510-089 in early 2012 and reported a BWB trend at the X-ray band. Prince et al. (2017) studied the long-term light curve of PKS 1510-089 at GeV bands and reported the BWB trend during flares in different campaigns. There are 14 outbursts/flares of individual TeV blazars that have been analyzed and their spectral behavior has been illustrated in Figure 4. 11 out of the 14 sources show the BWB trend, according to the insets in Figure 4, except 4FGL J0221.1+3556, 4FGL J0303.4–2407, and 4FGL J1512.8–0906. We suggest that this spectral behavior for blazars at the GeV band arises from the same mechanism, which is that the SSC process dominates the GeV emission for these TeV blazars. The nonthermal electrons produce the observed IC emission with an energy distribution of

$$\frac{dN}{d\gamma} = N_0 \gamma^{-\alpha}, \quad \gamma_{\min} \leq \gamma \leq \gamma_{\max}, \quad (8)$$

where  $\gamma$  is the Lorentz factor of electrons,  $\gamma_{\min}$  and  $\gamma_{\max}$  are the minimum and the maximum values of the Lorentz factor at the time of particle injection,  $N_0$  is related to the total particle density  $N_{\text{tot}}$  by  $N_0 = N_{\text{tot}}(1 - \alpha)/(\gamma_{\max}^{1-\alpha} - \gamma_{\min}^{1-\alpha})$ , and  $\alpha$  is the electron spectral index. Then, the SSC emissivity ( $j_{\text{ssc}}$ ) is related to the electron spectral index by

$$j_{\text{ssc}}(\epsilon) \sim \epsilon^{-(2+\alpha)/4}, \quad (9)$$

where  $\epsilon = h\nu/m_e c^2$  (Chiang & Böttcher 2002). From Equation (9), we can see that the spectral behavior at the GeV band for blazars is mainly determined by the shape of the electron spectrum, which means a harder electron spectrum results in a corresponding harder emission spectrum. In this case, we can obtain the electron spectral index through the GeV  $\gamma$ -ray photon index via  $-(\Gamma - 1) = -(2 + \alpha)/4$  for the 11 outbursts/flares and list the results in column (6) of Table 5.

## 5. Summary

This paper aims to provide detailed GeV variability of TeV blazars and study the GeV spectral behaviors. We performed an analysis using LAT data across 15 yr and offered annual GeV fluxes and corresponding photon spectral indices for the 78 TeV blazars in our sample. We calculated the detailed monthly flux and corresponding photon spectral index of the 41

bright TeV blazars to further investigate the spectral behavior. A series of variability property analyses were conducted on the fractional variability, flux distribution, flare duty cycle, PSDs, and periodic properties.

Our main conclusions are as follows:

1. We investigated the possible correlation between GeV luminosity and spectral photon index. The results suggest a strong correlation between the  $\log L_\gamma$  and  $\gamma$ -ray photon index for the FSRQs and HBLs, while there is no correlation for the IBLs.
2. There are 14 sources out of our sample that show significant flares, of which six exhibit a clear sharp peak profile in their 5 day binned light curves. 4FGL J0303.4–2407 and 4FGL J0739.2+0137 show fast-rising and slowly decaying subflares. This asymmetry can be related to the particle acceleration mechanism in the jet. While 4FGL J1751.5+0938 shows a slowly rising and fast-decaying subflare, which may be associated with an efficient cooling process.
3. We quantified the variability utilizing the fractional variability parameter  $F_{\text{var}}$  and the results indicate that the flux of the FSRQs showed significantly stronger variability than that of the BL Lacs. As the synchrotron peak frequency decreases, the  $F_{\text{var}}$  value generally becomes larger.
4. We constructed histograms of the observed GeV light curves and fitted them to two different PDFs, a normal distribution and a log-normal distribution. The results show that all of the bright sources in this work support a log-normal distribution.
5. Our duty cycle results of the monthly binned light curves show values ranging from 0.0–0.36, while the vast majority of the values are in the range of 0.0–0.2, except for three blazars.
6. We found that the periodograms are consistent with a power-law form with the slope index  $\beta$  ranging between 0.22 and 1.98. Our PSD result at the GeV band is slightly flatter and has a larger range compared with previous studies. In addition, 12 blazars in our sample have been reported to have high significance  $\gamma$ -ray QPOs.
7. Through checking the spectral behavior, we found 11 out of the 14 sources show a BWB trend, which suggests that this spectral behavior at the GeV band arises from the mechanism in which the SSC process dominates the GeV emission for these TeV blazars.

## Acknowledgments

Thanks are given to the reviewer for the constructive comments and suggestions that helped us make the paper more thorough. This work is supported by the National Natural Science Foundation of China (grants Nos. 11975072, 11835009, and 11805031), the National SKA Program of China (grant Nos. 2022SKA0110200 and 2022SKA0110203), and the 111 Project (grant No. B16009). G.W. acknowledges the support from the China Postdoctoral Science Foundation (grant No. 2023M730523). H.X. acknowledges the support from the National Natural Science Foundation of China (NSFC 12203034), from the Shanghai Science and Technology Fund (22YF1431500), and from the science research grants from the China Manned Space Project. J.F. is grateful for support from the NSFC (NSFC U2031201, NSFC 11733001), Scientific and

Technological Cooperation Projects (2020–2023) between the People's Republic of China and the Republic of Bulgaria, the Guangdong Major Project of Basic and Applied Basic Research (grant No. 2019B030302001), and the science research grants from the China Manned Space Project with No. CMSCSST-2021-A06.

### ORCID iDs

Gege Wang  <https://orcid.org/0000-0002-8032-4640>  
 Hubing Xiao  <https://orcid.org/0000-0001-8244-1229>  
 Junhui Fan  <https://orcid.org/0000-0002-5929-0968>  
 Xin Zhang  <https://orcid.org/0000-0002-6029-1933>

### References

- Abdo, A. A., Ackermann, M., Agudo, I., et al. 2010a, *ApJ*, 716, 30  
 Abdo, A. A., Ackermann, M., Agudo, I., et al. 2010b, *ApJ*, 721, 1425  
 Abdo, A. A., Ackermann, M., Ajello, M., et al. 2010c, *ApJ*, 722, 520  
 Abdo, A. A., Ajello, M., Allafort, A., et al. 2013, *ApJS*, 208, 17  
 Abdollahi, S., Acero, F., Ackermann, M., et al. 2020, *ApJS*, 247, 33  
 Abdollahi, S., Acero, F., Baldini, L., et al. 2022, *ApJS*, 260, 53  
 Abdollahi, S., Ackermann, M., Ajello, M., et al. 2017, *ApJ*, 846, 34  
 Abdollahi, S., Ajello, M., Baldini, L., et al. 2023, *ApJS*, 265, 31  
 Abeyskara, A. U., Archambault, S., Archer, A., et al. 2015, *ApJL*, 815, L22  
 Abeyskara, A. U., Archambault, S., Archer, A., et al. 2017a, *ApJ*, 836, 205  
 Abeyskara, A. U., Archambault, S., Archer, A., et al. 2017b, *ApJS*, 233, 7  
 Abeyskara, A. U., Archer, A., Benbow, W., et al. 2018, *ApJL*, 861, L20  
 Acciari, V. A., Aniello, T., Ansoldi, S., et al. 2022, *ApJ*, 927, 197  
 Acero, F., Ackermann, M., Ajello, M., et al. 2015, *ApJS*, 218, 23  
 Acharyya, A., Adams, C. B., Archer, A., et al. 2023, *ApJ*, 950, 152  
 Acharyya, A., Chadwick, P. M., & Brown, A. M. 2021, *MNRAS*, 500, 5297  
 Ackermann, M., Ajello, M., Albert, A., et al. 2015c, *ApJL*, 813, L41  
 Ackermann, M., Ajello, M., Allafort, A., et al. 2011, *ApJ*, 743, 171  
 Ackermann, M., Ajello, M., Atwood, W. B., et al. 2015, *ApJ*, 810, 14  
 Adams, C. B., Batshoun, J., Benbow, W., et al. 2022, *ApJ*, 924, 95  
 Ahnen, M. L., Ansoldi, S., Antonelli, L. A., et al. 2015, *ApJL*, 815, L23  
 Ahnen, M. L., Ansoldi, S., Antonelli, L. A., et al. 2016, *A&A*, 590, A24  
 Ajello, M., Angioni, R., Axelsson, M., et al. 2020, *ApJ*, 892, 105  
 Aleksić, J., Ansoldi, S., Antonelli, L. A., et al. 2014a, *A&A*, 572, A121  
 Aleksić, J., Ansoldi, S., Antonelli, L. A., et al. 2014b, *A&A*, 569, A46  
 Angioni, R. 2021, *ATel*, 14491, 1  
 Ansoldi, S., Antonelli, L. A., Arcaro, C., et al. 2018, *ApJL*, 863, L10  
 Archambault, S., Archer, A., Beilicke, M., et al. 2015, *ApJ*, 808, 110  
 Atwood, W. B., Abdo, A. A., Ackermann, M., et al. 2009, *ApJ*, 697, 1071  
 Ballet, J., Burnett, T. H., Digel, S. W., & Lott, B. 2020, arXiv:2005.11208  
 Benbow, W. & VERITAS Collaboration 2022, *ICRC (Berlin)*, 37, 794  
 Bhatta, G., & Dhital, N. 2020, *ApJ*, 891, 120  
 Bhatta, G., Stawarz, Ł., Ostrowski, M., et al. 2016, *ApJ*, 831, 92  
 Blanch, O. 2021, *ATel*, 14506, 1  
 Bloom, S. D., & Marscher, A. P. 1996, *ApJ*, 461, 657  
 Bonning, E., Urry, C. M., Bailyn, C., et al. 2012, *ApJ*, 756, 13  
 Catanese, M., Akerlof, C. W., Badran, H. M., et al. 1998, *ApJ*, 501, 616  
 Cavaliere, A., Tavani, M., & Vittorini, V. 2017, *ApJ*, 836, 220  
 Cerutti, M., Zech, A., Boisson, C., & Inoue, S. 2015, *MNRAS*, 448, 910  
 Chadwick, P. M., Lyons, K., McComb, T. J. L., et al. 1999, *ApJ*, 513, 161  
 Chatterjee, R., Bailyn, C. D., Bonning, E. W., et al. 2012, *ApJ*, 749, 191  
 Chen, L. 2018, *ApJS*, 235, 39  
 Chiang, J., & Böttcher, M. 2002, *ApJ*, 564, 92  
 Dai, B. Z., Li, X. H., Liu, Z. M., et al. 2009, *MNRAS*, 392, 1181  
 D'Ammando, F., Raiteri, C. M., Villata, M., et al. 2011, *A&A*, 529, A145  
 Dermer, C. D. 1999, *Aph*, 11, 1  
 Diltz, C., Böttcher, M., & Fossati, G. 2015, *ApJ*, 802, 133  
 Dimitrakoudis, S., Mastichiadis, A., Protheroe, R. J., & Reimer, A. 2012, *A&A*, 546, A120  
 Emery, G., Cerruti, M., Dmytriiev, A., et al. 2019, *ICRC (Madison)*, 36, 668  
 Eyer, L., & Bartholdi, P. 1999, *A&AS*, 135, 1  
 Fan, J. H. 1999, *MNRAS*, 308, 1032  
 Fan, J.-H., Bastieri, D., Yang, J.-H., et al. 2014, *RAA*, 14, 1135  
 Fan, J. H., Kurtanidze, S. O., Liu, Y., et al. 2021, *ApJS*, 253, 10  
 Fan, J. H., Yang, J. H., Liu, Y., et al. 2016, *ApJS*, 226, 20  
 Fan, J. H., Yang, J. H., Xiao, H. B., et al. 2017, *ApJL*, 835, L38  
 Finke, J. D., Dermer, C. D., & Böttcher, M. 2008, *ApJ*, 686, 181  
 Fiorucci, M., Ciprini, S., & Tosti, G. 2004, *A&A*, 419, 25  
 Fossati, G., Maraschi, L., Celotti, A., Comastri, A., & Ghisellini, G. 1998, *MNRAS*, 299, 433  
 Garrappa, S., Buson, S., Franckowiak, A., et al. 2019, *ApJ*, 880, 103  
 Ghisellini, G., Righi, C., Costamante, L., & Tavecchio, F. 2017, *MNRAS*, 469, 255  
 Gu, M. F., & Ai, Y. L. 2011, *A&A*, 528, A95  
 Gu, M. F., Lee, C. U., Pak, S., Yim, H. S., & Fletcher, A. B. 2006, *A&A*, 450, 39  
 Gupta, A. C., Agarwal, A., Bhagwan, J., et al. 2016, *MNRAS*, 458, 1127  
 H.E.S.S. Collaboration, Abdalla, H., Adam, R., et al. 2019, *A&A*, 627, A159  
 H.E.S.S. Collaboration, Abdalla, H., Adam, R., et al. 2020, *A&A*, 633, A162  
 H.E.S.S. Collaboration, Abdalla, H., Adam, R., et al. 2021, *A&A*, 648, A23  
 H.E.S.S. Collaboration, Abramowski, A., Acero, F., et al. 2013, *A&A*, 559, A136  
 Hayashida, M., Madejski, G. M., Nalewajko, K., et al. 2012, *ApJ*, 754, 114  
 Hayashida, M., Nalewajko, K., Madejski, G. M., et al. 2015, *ApJ*, 807, 79  
 Hayes, M., Schaerer, D., Östlin, G., et al. 2011, *ApJ*, 730, 8  
 Hirako, J., Terzic, T., Stamerra, A., et al. 2018, in Proc. of Science 329, Int. Conf. on Black Holes as Cosmic Batteries: UHECRs and Multimessenger Astronomy, ed. R. Cassia Anjos & C. H. Coimbra Araujo (Trieste: SISSA), 13  
 IceCube Collaboration, Aartsen, M. G., Ackermann, M., et al. 2018a, *Sci*, 361, 147  
 IceCube Collaboration, Aartsen, M. G., Ackermann, M., et al. 2018b, *Sci*, 361, eaat1378  
 Kang, S. J., Chen, L., & Wu, Q. W. 2014, *ApJS*, 215, 5  
 Komatsu, E., Smith, K. M., Dunkley, J., et al. 2011, *ApJS*, 192, 18  
 Kushwaha, P., Sinha, A., Misra, R., Singh, K. P., & de Gouveia Dal Pino, E. M. 2017, *ApJ*, 849, 138  
 Larionov, V. M., Villata, M., & Raiteri, C. M. 2010, *A&A*, 510, A93  
 Lomb, N. R. 1976, *Ap&SS*, 39, 447  
 MAGIC Collaboration, Acciari, V. A., Ansoldi, S., et al. 2020a, *A&A*, 640, A132  
 MAGIC Collaboration, Acciari, V. A., Ansoldi, S., et al. 2020b, *A&A*, 638, A14  
 MAGIC Collaboration, Acciari, V. A., & Ansoldi, S. 2021, *A&A*, 647, A163  
 MAGIC Collaboration, Ahnen, M. L., Ansoldi, S., et al. 2018, *A&A*, 617, A30  
 Meng, N., Zhang, X., Wu, J., Ma, J., & Zhou, X. 2018, *ApJS*, 237, 30  
 Meyer, M., Scargle, J. D., & Blandford, R. D. 2019, *ApJ*, 877, 39  
 Mücke, A., & Protheroe, R. J. 2001, *Aph*, 15, 121  
 Otero-Santos, J., Acosta-Pulido, J. A., Becerra González, J., et al. 2022, *MNRAS*, 511, 5611  
 Otero-Santos, J., Peñil, P., Acosta-Pulido, J. A., et al. 2023, *MNRAS*, 518, 5788  
 Ouyang, Z., Xiao, H., Chen, J., et al. 2023, *ApJ*, 949, 52  
 Paliya, V. S., Domínguez, A., Ajello, M., Olmo-García, A., & Hartmann, D. 2021, *ApJS*, 253, 46  
 Peñil, P., Ajello, M., Buson, S., et al. 2022, arXiv:2211.01894  
 Peñil, P., Domínguez, A., Buson, S., et al. 2020, *ApJ*, 896, 134  
 Pittori, C., Lucarelli, F., Verrecchia, F., et al. 2018, *ApJ*, 856, 99  
 Prince, R., Majumdar, P., & Gupta, N. 2017, *ApJ*, 844, 62  
 Prokhorov, D. A., & Moraghan, A. 2017, *MNRAS*, 471, 3036  
 Punch, M., Akerlof, C. W., Cawley, M. F., et al. 1992, *Natur*, 358, 477  
 Quinn, J., Akerlof, C. W., Biller, S., et al. 1996, *ApJL*, 456, L83  
 Raiteri, C. M., Villata, M., Acosta-Pulido, J. A., et al. 2017, *Natur*, 552, 374  
 Rani, B., Gupta, A. C., Strigachev, A., et al. 2010, *MNRAS*, 404, 1992  
 Ren, H. X., Cerruti, M., & Sahakyan, N. 2023, *A&A*, 672, A86  
 Safna, P. Z., Stalin, C. S., Rakshit, S., & Mathew, B. 2020, *MNRAS*, 498, 3578  
 Scargle, J. D. 1982, *ApJ*, 263, 835  
 Scarpa, R., & Falomo, R. 1997, *A&A*, 325, 109  
 Schüssler, F., Seglar-Arroyo, M., Arrieta, M., et al. 2017, *ICRC (Busan)*, 35, 652  
 Shah, Z., Mankuzhiyil, N., Sinha, A., et al. 2018, *RAA*, 18, 141  
 Shieh, G. S. 1998, *Stat. Probab. Lett.*, 39, 17  
 Shukla, A., & Mannheim, K. 2020, *NatCo*, 11, 4176  
 Sikora, M., Begelman, M. C., & Rees, M. J. 1994, *ApJ*, 421, 153  
 Singh, K. K., & Meintjes, P. J. 2020, *AN*, 341, 713  
 Sinha, A., Sahayanathan, S., Acharya, B. S., et al. 2017, *ApJ*, 836, 83  
 Sobacchi, E., Sormani, M. C., & Stamerra, A. 2017, *MNRAS*, 465, 161  
 Sobolewska, M. A., Siemiginowska, A., Kelly, B. C., & Nalewajko, K. 2014, *ApJ*, 786, 143  
 Sokolov, A., Marscher, A. P., & McHardy, I. M. 2004, *ApJ*, 613, 725  
 Spada, M., Ghisellini, G., Lazzati, D., & Celotti, A. 2001, *MNRAS*, 325, 1559  
 Tanaka, Y. T., Becerra Gonzalez, J., Itoh, R., et al. 2016, *PASJ*, 68, 51

- Tarnopolski, M., Żywucka, N., Marchenko, V., & Pascual-Granado, J. 2020, *ApJS*, **250**, 1
- Tolamatti, A., Ghosal, B., Singh, K. K., et al. 2022, *APh*, **139**, 102687
- Urry, C. M. 1996, in ASP Conf. Ser. 110, Blazar Continuum Variability, ed. H. R. Miller, J. R. Webb, & J. C. Noble (San Francisco, CA: ASP), 391
- Urry, C. M., & Padovani, P. 1995, *PASP*, **107**, 803
- VanderPlas, J. T. 2018, *ApJS*, **236**, 16
- Vaughan, S., Edelson, R., Warwick, R. S., & Uttley, P. 2003, *MNRAS*, **345**, 1271
- Villata, M., Raiteri, C. M., Balonek, T. J., et al. 2006, *A&A*, **453**, 817
- Wagner, S. J. 2020, *ATel*, **13632**, 1
- Wang, G., Fan, J., Xiao, H., & Cai, J. 2022a, *PASP*, **134**, 104101
- Wang, G. G., Cai, J. T., & Fan, J. H. 2022b, *ApJ*, **929**, 130
- Wang, N., Yi, T.-F., Wang, L., et al. 2023, *RAA*, **23**, 115011
- Wang, Z.-R., Liu, R.-Y., Petropoulou, M., et al. 2022c, *PhRvD*, **105**, 023005
- Webb, J. R., Arroyave, V., Laurence, D., et al. 2021, *Galax*, **9**, 114
- Xiao, H., Fan, J., Yang, J., et al. 2019, *SCPMA*, **62**, 129811
- Xiao, H., Ouyang, Z., Zhang, L., et al. 2022a, *ApJ*, **925**, 40
- Xiao, H. B., Zhu, J. T., Fan, J. H., et al. 2022b, *MNRAS*, **517**, 4202
- Xiong, D., Bai, J., Fan, J., et al. 2020, *ApJS*, **247**, 49
- Xue, R., Liu, R.-Y., Wang, Z.-R., Ding, N., & Wang, X.-Y. 2021, *ApJ*, **906**, 51
- Yang, J. H., Fan, J. H., Liu, Y., et al. 2022, *ApJS*, **262**, 18
- Yoshida, K., Petropoulou, M., Murase, K., & Oikonomou, F. 2023, *ApJ*, **954**, 194
- Yuan, Y.-H., Fan, J.-h., Tao, J., et al. 2017, *A&A*, **605**, A43
- Yuan, Y. H., Wang, G. G., Xiao, H. B., et al. 2022, *ApJS*, **262**, 43
- Zacharias, M., Dominis Prester, D., Jankowsky, F., et al. 2019, *Galax*, **7**, 41
- Zhang, B.-K., Zhao, X.-Y., & Wu, Q. 2022, *ApJS*, **259**, 49
- Zhang, Y. H., Treves, A., Celotti, A., et al. 2002, *ApJ*, **572**, 762